1.3 Numerical Simulation of Marangoni Convection in Consideration of Free Surface Displacement (Part4)

Hiroshi Kawamura

Science University of Tokyo

NUMERICAL SIMULATION OF MARANGONI CONVECTION IN CONSIDERATION OF FREE SURFACE DISPLACEMENT(PART 4)

Masayuki Goto*, Kenichi Shida*, Hiroshi Kawamura* and Shinichi Yoda**

***Science University of Tokyo, 2641 Yamazaki, Noda-shi, Chiba 278-8510, Japan**

****National Space Development Agency of Japan, 2-1-1 Sengen, Tsukuba City, 305-8505, Japan**

Numerical simulation concerning the thermocapillary convection in a half-zone liquid bridge taken static and dynamic surface deformation into account was conducted. The liquid bridge has a free surface, which deforms due to the thermocapillary-driven flow as well as the gravity. In this research, the fundamental equations and the boundary conditions were derived for the concerned configuration with taking the static axisymmetric and for the dynamic 3-D free-surface displacement into account. Then, (1) code validation concerning the moderate Prandtl number fluid and (2) a series of analysis concerning the high Prandtl number fluid were conducted. In the code validation the critical Marangoni number and the fundamental frequency of the induced flow were in good agreement with those obtained by linear stability analysis. As for the analysis concerning the high Prandtl number fluid, the critical Marangoni number with and without considering the dynamic surface deformation was obtained. In addition, the phase differences among the surface deformation, the axis- and azimuthal-velocity, and the surface temperature variation were analyzed. It was found that the rotating oscillatory flow retained a lower fundamental frequency than the pulsating one, which was also indicated by the terrestrial experiments.

1 INTRODUCTION

One of the purposes of the space environment utilization such as a space station is the production of a new material. Uniform or high-quality material can rather hardly be formed on the ground owing to the natural convection by the buoyancy effect and sedimentation by the density difference. On the other hand, the buoyancy effect can be reduced and thus, a high-quality material processing is expected to be enabled in the space environment.

Floating Zone Method is one of the likely candidates of the material processing methods under the micro-gravity. In this method the both ends of the material rod are cooled down, and the center is heated to be melt. Molten liquid sustained between the rods is called a liquid bridge. This melt zone is slowly moved vertically and thus a uniform single crystal is produced. The material in the liquid phase is sustained by the surface tension. Generally the surface tension of a liquid decreases with increasing temperature. Because a temperature gradient exists along the free surface, the difference of the surface tension is originated by the temperature difference. Thus a flow occurs in a liquid bridge even under the micro-gravity. This flow is called as thermocapillary or Marangoni convection. Though this convection can occur also on the ground, it is usually hidden by the buoyancy. Thus this phenomenon is hardly recognized in our usual observation. On the other

hand, thermocapillary convection becomes dominant under the micro-gravity because the influence of the buoyancy is strongly reduced. Therefore, the analysis of the thermocapillary convection is of primary importance for the material formation under the micro-gravity. The configuration of the floating zone method is called as Full Zone Model. The upper half of the full zone model is deeply influenced by the buoyancy on the ground so that the thermocapillary effect can scarcely be recognized. On the other hand, the lower half is less affected by buoyancy. Because upper temperature is higher than the lower one. As the results the thermocapillary effect dominates the convection in the lower half of the full zone model. Consequently Half Zone Model is preferred in the fundamental research on the ground and is employed in this research as well. The half zone model corresponds to the half part of the liquid bridge in the full zone model; the one side of the bridge is heated up and the other is cooled down.

The experiments for the thermocapillary convention are widely conducted. Kamotani[1] studied effect of zone rotation on oscillatory thermocapillary flow in simulated floating zones. Velten[2] observed the periodic instability of thermocapillary convection in cylindrical liquid bridges.

As for the numerical simulation Savino and Monti[3] simulated the oscillatory flow numerically and compared it with their experiments. Yasuhiro[4] investigated the relations between the wave number and aspect ratio or Marangoni number.

From these researches, it turned out that thermocapillary convection exhibits the oscillatory flow under a certain condition.

It should be noted that the existing numerical simulations ware conducted without considering the free surface movement. On the other hand, the free surface vibration is observed with the oscillatory flow in the terrestrial experiments. An influence of surface vibration upon the flow field instability must be evaluated to understand the mechanism of the oscillatory flow.

Consequently the purpose of this research is to analyze the three dimensional thermocapillary convection numerically with consideration of the free surface movement.

2 NUMERICAL METHOD FOR THE THREE DIMENSIONAL ANALYSIS

The goal of this study is to analyze the influence of the free surface deformation upon the thermocapillary flow. Therefore, an analytical method is developed to capture the temporally varing surface motion. In this analysis, B.F.C.(Boundary Fitted Coordinate) method is employed.

2.1 The governing equation

[Continuity equation]

$$\frac{\partial}{\partial r}(rv_r) + \frac{\partial v_\theta}{\partial \theta} + \frac{\partial}{\partial z}(rv_z) = 0 \tag{1}$$

[Navier-Stokes equation]
(r-direction)

$$r\frac{\partial v_r}{\partial t} + \frac{\partial}{\partial r}(rv_r v_r) + \frac{\partial}{\partial \theta}(v_\theta v_r) - v_\theta^2 + \frac{\partial}{\partial z}(rv_z v_r) = -r\frac{\partial P}{\partial r}$$

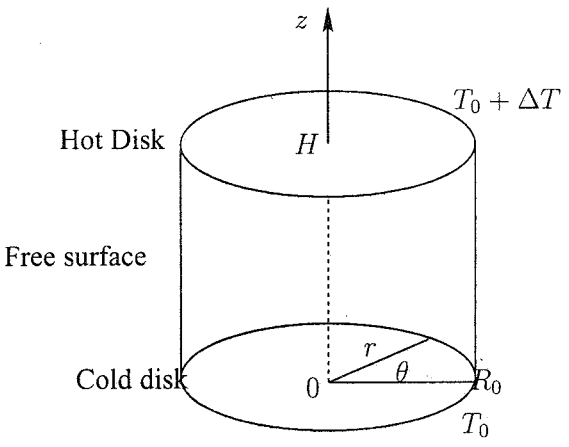

Figure 1: The configuration

To consider a thermocapillary convection in a liquid bridge, a configuration of the analysis is defined in figure 1. The liquid bridge with volume V is bounded by two rigid parallel disks of equal radii $r = R_0$ located at $z = 0$ and H.
The temperature difference between these disks is defined by ΔT. The gravity is assumed in the direction of $-z$.
The governing equations are described in cylindrical coordinate. As for the gravity, the Oberbeck-Boussinesq approximation is utilized in these equations.

$$+\frac{Pr}{Ma}[\frac{\partial}{\partial r}(r\frac{\partial v_r}{\partial r}) + \frac{\partial}{\partial \theta}(\frac{1}{r}\frac{\partial v_r}{\partial \theta}) + \frac{\partial}{\partial z}(r\frac{\partial v_r}{\partial z}) - \frac{v_r}{r} - \frac{2}{r}\frac{\partial v_\theta}{\partial \theta}]$$

(θ-direction)

$$r\frac{\partial v_\theta}{\partial t} + \frac{\partial}{\partial r}(rv_r v_\theta) + \frac{\partial}{\partial \theta}(v_\theta v_\theta) - v_r v_\theta + \frac{\partial}{\partial z}(rv_z v_\theta) = -\frac{\partial P}{\partial \theta}$$
$$+\frac{Pr}{Ma}[\frac{\partial}{\partial r}(r\frac{\partial v_\theta}{\partial r}) + \frac{\partial}{\partial \theta}(\frac{1}{r}\frac{\partial v_\theta}{\partial \theta}) + \frac{\partial}{\partial z}(r\frac{\partial v_\theta}{\partial z}) + \frac{2}{r}\frac{\partial v_r}{\partial \theta} - \frac{v_\theta}{r}]$$

(z-direction)

$$r\frac{\partial v_z}{\partial t} + \frac{\partial}{\partial r}(rv_r v_z) + \frac{\partial}{\partial \theta}(v_\theta v_z) + \frac{\partial}{\partial z}(rv_z v_z) = -\frac{\partial P}{\partial z}$$
$$+\frac{Pr}{Ma}[\frac{\partial}{\partial r}(r\frac{\partial v_z}{\partial r}) + \frac{\partial}{\partial \theta}(\frac{1}{r}\frac{\partial v_z}{\partial \theta}) + \frac{\partial}{\partial z}(r\frac{\partial v_z}{\partial z})]$$
$$+\frac{Gr}{Re^2}T \qquad (2)$$

[Energy equation]

$$r\frac{\partial T}{\partial t} + \frac{\partial}{\partial r}(rv_r T) + \frac{\partial}{\partial \theta}(v_\theta T) + \frac{\partial}{\partial z}(rv_z T)$$
$$= \frac{1}{Ma}[\frac{\partial}{\partial r}(r\frac{\partial T}{\partial r}) + \frac{\partial}{\partial \theta}(\frac{1}{r}\frac{\partial T}{\partial \theta}) + \frac{\partial}{\partial z}(r\frac{\partial T}{\partial z})] \qquad (3)$$

The scales used for non-dimensionalization are as follows.

Table 1: Scales used for non-dimensionalization

Variable	r, z	t	v $= (v_r, v_\theta, v_z)$	p	T
Scale	H	$H\mu/\sigma_T\Delta T$	$\sigma_T\Delta T/\mu$	$\rho(\sigma_T\Delta T/\mu)^2$	ΔT

The non-dimensional numbers are defined by

$$Re = \frac{vH}{\nu}$$

$$
\begin{aligned}
Pr &= \frac{\nu}{\kappa} \\
Ma &= \frac{1}{\mu\kappa}\sigma_T \Delta T \cdot H \\
Gr &= \frac{g\beta\Delta T H^3}{\nu^2}
\end{aligned}
$$

Eqs. (1)-(3) can be transformed from the physical domain to the computational domain by Jacobian matrix.

$$
\begin{bmatrix} \frac{\partial}{\partial t} \\ \frac{\partial}{\partial r} \\ \frac{\partial}{\partial \theta} \\ \frac{\partial}{\partial z} \end{bmatrix} = \begin{bmatrix} 1 & \xi_t & \zeta_t & \eta_t \\ 0 & \xi_r & \zeta_r & \eta_r \\ 0 & \xi_\theta & \zeta_\theta & \eta_\theta \\ 0 & \xi_z & \zeta_z & \eta_z \end{bmatrix} \begin{bmatrix} \frac{\partial}{\partial \tau} \\ \frac{\partial}{\partial \xi} \\ \frac{\partial}{\partial \zeta} \\ \frac{\partial}{\partial \eta} \end{bmatrix} \tag{4}
$$

$$
\begin{bmatrix} \frac{\partial}{\partial \tau} \\ \frac{\partial}{\partial \xi} \\ \frac{\partial}{\partial \zeta} \\ \frac{\partial}{\partial \eta} \end{bmatrix} = \begin{bmatrix} 1 & r_\tau & \theta_\tau & z_\tau \\ 0 & r_\xi & \theta_\xi & z_\xi \\ 0 & r_\zeta & \theta_\zeta & z_\zeta \\ 0 & r_\eta & \theta_\eta & z_\eta \end{bmatrix} \begin{bmatrix} \frac{\partial}{\partial t} \\ \frac{\partial}{\partial r} \\ \frac{\partial}{\partial \theta} \\ \frac{\partial}{\partial z} \end{bmatrix} \tag{5}
$$

Equation (5) is inversely transformed as follows,

$$
\begin{bmatrix} \frac{\partial}{\partial t} \\ \frac{\partial}{\partial r} \\ \frac{1}{r}\frac{\partial}{\partial \theta} \\ \frac{\partial}{\partial z} \end{bmatrix} = \frac{1}{J} \begin{bmatrix} A_{11} & A_{12} & A_{13} & A_{14} \\ A_{21} & A_{22} & A_{23} & A_{24} \\ A_{31} & A_{32} & A_{33} & A_{34} \\ A_{41} & A_{42} & A_{43} & A_{44} \end{bmatrix} \begin{bmatrix} \frac{\partial}{\partial \tau} \\ \frac{\partial}{\partial \xi} \\ \frac{1}{\xi}\frac{\partial}{\partial \zeta} \\ \frac{\partial}{\partial \eta} \end{bmatrix} \tag{6}
$$

$$
\begin{aligned}
A_{11} &= \frac{r}{\xi}(r_\xi\theta_\zeta z_\eta + r_\zeta\theta_\eta z_\xi + r_\eta\theta_\xi z_\zeta - r_\eta\theta_\zeta z_\xi - r_\zeta\theta_\xi z_\eta - r_\xi\theta_\eta z_\zeta) \\
A_{12} &= -\frac{r}{\xi}(r_\tau\theta_\zeta z_\eta + r_\zeta\theta_\eta z_\tau + r_\eta\theta_\tau z_\zeta - r_\eta\theta_\zeta z_\tau - r_\zeta\theta_\tau z_\eta - r_\tau\theta_\eta z_\zeta) \\
A_{13} &= r(r_\tau\theta_\xi z_\eta + r_\xi\theta_\eta z_\tau + r_\eta\theta_\tau z_\xi - r_\eta\theta_\xi z_\tau - r_\xi\theta_\tau z_\eta - r_\tau\theta_\eta z_\xi) \\
A_{14} &= -\frac{r}{\xi}(r_\tau\theta_\xi z_\zeta + r_\xi\theta_\zeta z_\tau + r_\zeta\theta_\tau z_\xi - r_\zeta\theta_\xi z_\tau - r_\xi\theta_\tau z_\zeta - r_\tau\theta_\zeta z\xi) \\
A_{21} &= 0 \\
A_{22} &= \frac{r}{\xi}(\theta_\zeta z_\eta - \theta_\eta z_\zeta) \\
A_{23} &= -r(\theta_\xi z_\eta - \theta_\eta z_\xi) \\
A_{24} &= \frac{r}{\xi}(\theta_\xi z_\zeta - \theta_\zeta z_\xi) \\
A_{31} &= 0 \\
A_{32} &= -\frac{1}{\xi}(r_\zeta z_\eta - r_\eta z_\zeta) \\
A_{33} &= (r_\xi z_\eta - r_\eta z_\xi) \\
A_{34} &= -\frac{1}{\xi}(r_\xi z_\zeta - r_\zeta z_\xi) \\
A_{41} &= 0
\end{aligned}
$$

$$A_{42} = \frac{r}{\xi}(r_\zeta\theta_\eta - r_\eta\theta_\zeta)$$
$$A_{43} = -r(r_\xi\theta_\eta - r_\eta\theta_\xi)$$
$$A_{44} = \frac{r}{\xi}(r_\xi\theta_\zeta - r_\zeta\theta_\xi)$$

Each component can be related from Eqs. (4), (6) as:

$$J = \frac{r}{\xi}(r_\xi\theta_\zeta z_\eta + r_\zeta\theta_\eta z_\xi + r_\eta\theta_\xi z_\zeta - r_\eta\theta_\zeta z_\xi - r_\zeta\theta_\xi z_\eta - r_\xi\theta_\eta z_\zeta)$$
$$\xi_t = -\frac{1}{J}\frac{r}{\xi}(r_\tau\theta_\zeta z_\eta + r_\zeta\theta_\eta z_\tau + r_\eta\theta_\tau z_\zeta - r_\eta\theta_\zeta z_\tau - r_\zeta\theta_\tau z_\eta - r_\tau\theta_\eta z_\zeta)$$
$$\zeta_t = \frac{1}{J}r(r_\tau\theta_\xi z_\eta + r_\xi\theta_\eta z_\tau + r_\eta\theta_\tau z_\xi - r_\eta\theta_\xi z_\tau - r_\xi\theta_\tau z_\eta - r_\tau\theta_\eta z_\xi)$$
$$\eta_t = -\frac{1}{J}\frac{r}{\xi}(r_\tau\theta_\xi z_\zeta + r_\xi\theta_\zeta z_\tau + r_\zeta\theta_\tau z_\xi - r_\zeta\theta_\xi z_\tau - r_\xi\theta_\tau z_\zeta - r_\tau\theta_\zeta z\xi)$$
$$\xi_r = \frac{1}{J}\frac{r}{\xi}(\theta_\zeta z_\eta - \theta_\eta z_\zeta)$$
$$\zeta_r = -\frac{1}{J}r(\theta_\xi z_\eta - \theta_\eta z_\xi)$$
$$\eta_r = \frac{1}{J}\frac{r}{\xi}(\theta_{xi} z\zeta - \theta_\zeta z_\xi)$$
$$\xi_\theta = -\frac{1}{J}\frac{1}{\xi}(r_\zeta z_\eta - r_\eta z_\zeta)$$
$$\zeta_\theta = \frac{1}{J}(r_\xi z_\eta - r_\eta z_\xi)$$
$$\eta_\theta = -\frac{1}{J}\frac{1}{\xi}(r_\xi z_\zeta - r_\zeta z_\xi)$$
$$\xi_z = \frac{1}{J}\frac{r}{\xi}(r_\zeta\theta_\eta - r_\eta\theta_\zeta)$$
$$\zeta_z = -\frac{1}{J}r(r_\xi\theta_\eta - r_\eta\theta_\xi)$$
$$\eta_z = \frac{1}{J}\frac{r}{\xi}(r_\xi\theta_\zeta - r_\zeta\theta_\xi)$$

The continuity equation, the Navier-Stokes equation and the energy equation (Eqs. (1)-(3)) are transformed by these rules.
[Continuity equation]

$$\frac{1}{\xi}\frac{\partial}{\partial\xi}(J\xi V_\xi) + \frac{1}{\xi}\frac{\partial}{\partial\zeta}(JV_\zeta) + \frac{\partial}{\partial\eta}(JV_\eta) = 0 \tag{7}$$

Here, V_ξ, V_ζ, V_η are defined by

$$V_\xi = \xi_r v_r + \frac{1}{r}\xi_\theta v_\theta + \xi_z v_z$$
$$V_\zeta = \xi\zeta_r v_r + \frac{\xi}{r}\zeta_\theta v_\theta + \xi\zeta_z v_z$$
$$V_\eta = \eta_r v_r + \frac{1}{r}\eta_\theta v_\theta + \eta_z v_z \,.$$

These velocities are called as **contravariant velocities**.
[Navier-Stokes equation]

$$\frac{\partial v_i}{\partial t} + (\mathbf{U}\cdot\nabla)v_i = \nabla P + \frac{Pr}{Ma}\nabla^2 v_i + e_z\frac{Gr}{Re^2}T \tag{8}$$

Equation (8) is expanded as

$$\begin{aligned}
&\frac{\partial v_i}{\partial t} + \xi_t\frac{\partial v_i}{\partial \xi} + \zeta_t\frac{\partial v_i}{\partial \zeta} + \eta_t\frac{\partial v_i}{\partial \eta} \\
&+\frac{1}{J}\Big[\frac{1}{\xi}\frac{\partial}{\partial \xi}(J\xi V_\xi v_i) + \frac{1}{\xi}\frac{\partial}{\partial \zeta}(JV_\zeta v_i) + \frac{\partial}{\partial \eta}(JV_\eta v_i) + e_r\Big(-\frac{Jv_\theta^2}{r}\Big) + e_\theta\Big(\frac{Jv_r v_\theta}{r}\Big)\Big] \\
= \quad & -\Big(\xi_i\frac{\partial P}{\partial \xi} + \zeta_i\frac{\partial P}{\partial \zeta} + \eta_i\frac{\partial P}{\partial \eta}\Big)e_i \\
+\frac{Pr}{Ma}\frac{1}{J}\Big[\quad & \frac{1}{\xi}\frac{\partial}{\partial \xi}(J\xi\xi_r\xi_r\frac{\partial v_i}{\partial \xi}) + \frac{1}{\xi}\frac{\partial}{\partial \xi}(J\xi\xi_r\zeta_r\frac{\partial v_i}{\partial \zeta}) + \frac{1}{\xi}\frac{\partial}{\partial \xi}(J\xi\xi_r\eta_r\frac{\partial v_i}{\partial \eta}) \\
+ \quad & \frac{1}{\xi}\frac{\partial}{\partial \zeta}(J\xi\zeta_r\xi_r\frac{\partial v_i}{\partial \xi}) + \frac{\partial}{\partial \zeta}(J\xi\zeta_r\zeta_r\frac{\partial v_i}{\partial \zeta}) + \frac{\partial}{\partial \zeta}(J\xi\zeta_r\eta_r\frac{\partial v_i}{\partial \eta}) \\
+ \quad & \frac{\partial}{\partial \eta}(J\eta_r\xi_r\frac{\partial v_i}{\partial \xi}) + \frac{\partial}{\partial \eta}(J\eta_r\zeta_r\frac{\partial v_i}{\partial \zeta}) + \frac{\partial}{\partial \eta}(J\eta_r\eta_r\frac{\partial v_i}{\partial \eta}) \\
+ \quad & \frac{\partial}{\partial \xi}(J\frac{1}{r^2}\xi_\theta\xi_\theta\frac{\partial v_i}{\partial \xi}) + \frac{\partial}{\partial \xi}(J\frac{1}{r^2}\xi_\theta\zeta_\theta\frac{\partial v_i}{\partial \zeta}) + \frac{\partial}{\partial \xi}(J\frac{1}{r^2}\xi_\theta\eta_\theta\frac{\partial v_i}{\partial \eta}) \\
+ \quad & \frac{1}{\xi}\frac{\partial}{\partial \zeta}(J\frac{\xi}{r^2}\zeta_\theta\xi_\theta\frac{\partial v_i}{\partial \xi}) + \frac{1}{\xi}\frac{\partial}{\partial \zeta}(J\frac{\xi}{r^2}\zeta_\theta\zeta_\theta\frac{\partial v_i}{\partial \zeta}) + \frac{1}{\xi}\frac{\partial}{\partial \zeta}(J\frac{\xi}{r^2}\zeta_\theta\eta_\theta\frac{\partial v_i}{\partial \eta}) \\
+ \quad & \frac{\partial}{\partial \eta}(J\frac{1}{r^2}\eta_\theta\xi_\theta\frac{\partial v_i}{\partial \xi}) + \frac{\partial}{\partial \eta}(J\frac{1}{r^2}\eta_\theta\zeta_\theta\frac{\partial v_i}{\partial \zeta}) + \frac{\partial}{\partial \eta}(J\frac{1}{r^2}\eta_\theta\eta_\theta\frac{\partial v_i}{\partial \eta}) \\
+ \quad & \frac{1}{\xi}\frac{\partial}{\partial \xi}(J\xi\xi_z\xi_z\frac{\partial v_i}{\partial \xi}) + \frac{\partial}{\partial \xi}(J\xi\xi_z\zeta_z\frac{\partial v_i}{\partial \zeta}) + \frac{\partial}{\partial \xi}(J\xi\xi_z\eta_z\frac{\partial v_i}{\partial \eta}) \\
+ \quad & \frac{1}{\xi}\frac{\partial}{\partial \zeta}(J\xi\zeta_z\xi_z\frac{\partial v_i}{\partial \xi}) + \frac{\partial}{\partial \zeta}(J\xi\zeta_z\zeta_z\frac{\partial v_i}{\partial \zeta}) + \frac{\partial}{\partial \zeta}(J\xi\zeta_z\eta_z\frac{\partial v_i}{\partial \eta}) \\
+ \quad & \frac{\partial}{\partial \eta}(J\eta_z\xi_z\frac{\partial v_i}{\partial \xi}) + \frac{\partial}{\partial \eta}(J\eta_z\zeta_z\frac{\partial v_i}{\partial \zeta}) + \frac{\partial}{\partial \eta}(J\eta_z\eta_z\frac{\partial v_i}{\partial \eta}) \\
+ \quad & e_r\Big(-J\frac{v_r}{r^2} - J\frac{2}{r^2}\Big(\frac{1}{r}\xi_\theta\frac{\partial v_\theta}{\partial \xi} + \frac{1}{r}\zeta_\theta\frac{\partial v_\theta}{\partial \zeta} + \frac{1}{r}\eta_\theta\frac{\partial v_\theta}{\partial \eta}\Big)\Big) \\
+ \quad & e_\theta\Big(-J\frac{v_\theta}{r^2} + J\frac{2}{r^2}\Big(\frac{1}{r}\xi_\theta\frac{\partial v_r}{\partial \xi} + \frac{1}{r}\zeta_\theta\frac{\partial v_r}{\partial \zeta} + \frac{1}{r}\eta_\theta\frac{\partial v_r}{\partial \eta}\Big)\Big)\Big] \\
+ \quad & e_z\Big(\frac{Gr}{Re^2}T\Big),
\end{aligned} \tag{9}$$

where $v_i = (v_r, v_\theta, v_z)$.
[Energy equation]

$$\frac{\partial T}{\partial t} + (\mathbf{U}\cdot\nabla)T = \frac{1}{Ma}\nabla^2 T \tag{10}$$

Equation (10) is expanded as equation (11).

$$\frac{\partial T}{\partial t} + \xi_t\frac{\partial T}{\partial \xi} + \zeta_t\frac{\partial T}{\partial \zeta} + \eta_t\frac{\partial T}{\partial \eta}$$

$$
\begin{aligned}
&+\frac{1}{J}\Big[\frac{1}{\xi}\frac{\partial}{\partial\xi}(J\xi V_\xi T)+\frac{1}{\xi}\frac{\partial}{\partial\zeta}(JV_\zeta T)+\frac{\partial}{\partial\eta}(JV_\eta T)\Big]\\
+\tfrac{1}{Ma}\tfrac{1}{J}\Big[\;&\frac{1}{\xi}\frac{\partial}{\partial\xi}(J\xi\xi_r\xi_r\frac{\partial T}{\partial\xi})+\frac{1}{\xi}\frac{\partial}{\partial\xi}(J\xi\xi_r\zeta_r\frac{\partial T}{\partial\zeta})+\frac{1}{\xi}\frac{\partial}{\partial\xi}(J\xi\xi_r\eta_r\frac{\partial T}{\partial\eta})\\
+\;&\frac{1}{\xi}\frac{\partial}{\partial\zeta}(J\xi\zeta_r\xi_r\frac{\partial T}{\partial\xi})+\frac{\partial}{\partial\zeta}(J\xi\zeta_r\zeta_r\frac{\partial T}{\partial\zeta})+\frac{\partial}{\partial\zeta}(J\xi\zeta_r\eta_r\frac{\partial T}{\partial\eta})\\
+\;&\frac{\partial}{\partial\eta}(J\eta_r\xi_r\frac{\partial T}{\partial\xi})+\frac{\partial}{\partial\eta}(J\eta_r\zeta_r\frac{\partial T}{\partial\zeta})+\frac{\partial}{\partial\eta}(J\eta_r\eta_r\frac{\partial T}{\partial\eta})\\
+\;&\frac{\partial}{\partial\xi}(J\frac{1}{r^2}\xi_\theta\xi_\theta\frac{\partial T}{\partial\xi})+\frac{\partial}{\partial\xi}(J\frac{1}{r^2}\xi_\theta\zeta_\theta\frac{\partial T}{\partial\zeta})+\frac{\partial}{\partial\xi}(J\frac{1}{r^2}\xi_\theta\eta_\theta\frac{\partial T}{\partial\eta})\\
+\;&\frac{1}{\xi}\frac{\partial}{\partial\zeta}(J\frac{\xi}{r^2}\zeta_\theta\xi_\theta\frac{\partial T}{\partial\xi})+\frac{1}{\xi}\frac{\partial}{\partial\zeta}(J\frac{\xi}{r^2}\zeta_\theta\zeta_\theta\frac{\partial T}{\partial\zeta})+\frac{1}{\xi}\frac{\partial}{\partial\zeta}(J\frac{\xi}{r^2}\zeta_\theta\eta_\theta\frac{\partial T}{\partial\eta})\\
+\;&\frac{\partial}{\partial\eta}(J\frac{1}{r^2}\eta_\theta\xi_\theta\frac{\partial T}{\partial\xi})+\frac{\partial}{\partial\eta}(J\frac{1}{r^2}\eta_\theta\zeta_\theta\frac{\partial T}{\partial\zeta})+\frac{\partial}{\partial\eta}(J\frac{1}{r^2}\eta_\theta\eta_\theta\frac{\partial T}{\partial\eta})\\
+\;&\frac{1}{\xi}\frac{\partial}{\partial\xi}(J\xi\xi_z\xi_z\frac{\partial T}{\partial\xi})+\frac{\partial}{\partial\xi}(J\xi\xi_z\zeta_z\frac{\partial T}{\partial\zeta})+\frac{\partial}{\partial\xi}(J\xi\xi_z\eta_z\frac{\partial T}{\partial\eta})\\
+\;&\frac{1}{\xi}\frac{\partial}{\partial\zeta}(J\xi\zeta_z\xi_z\frac{\partial T}{\partial\xi})+\frac{\partial}{\partial\zeta}(J\xi\zeta_z\zeta_z\frac{\partial T}{\partial\zeta})+\frac{\partial}{\partial\zeta}(J\xi\zeta_z\eta_z\frac{\partial T}{\partial\eta})\\
+\;&\frac{\partial}{\partial\eta}(J\eta_z\xi_z\frac{\partial T}{\partial\xi})+\frac{\partial}{\partial\eta}(J\eta_z\zeta_z\frac{\partial T}{\partial\zeta})+\frac{\partial}{\partial\eta}(J\eta_z\eta_z\frac{\partial T}{\partial\eta})\Big]
\end{aligned}
\tag{11}
$$

2.2 The coupling and time advancement

In this analysis, fractional step method is utilized to computate these governing equations. Euler method is adapted for time advancement.
Here, the time in the computational domain is defined as the same time in the physical domain ($\tau = t$).
Equation (9) is described as

$$
\frac{\partial v_i}{\partial\tau}+f_t+f_c=-\Big(\xi_i\frac{\partial P}{\partial\xi}+\zeta_i\frac{\partial P}{\partial\zeta}+\eta_i\frac{\partial P}{\partial\eta}\Big)e_i+f_v\,, \tag{12}
$$

where f_t, f_c and f_v are the coordinate movement, convection and viscosity terms, respectively.
In fractional step method, the velocity is solved by dividing into three steps as below.

$$
\tilde{v_i} = v_i^{(n)}+\Delta t\cdot\{-f_c+f_v\} \tag{13}
$$

$$
\hat{v_i} = \tilde{v_i}-\Delta t\cdot\Big(\xi_i\frac{\partial P^{(n+1)}}{\partial\xi}+\zeta_i\frac{\partial P^{(n+1)}}{\partial\zeta}+\eta_i\frac{\partial P^{(n+1)}}{\partial\eta}\Big)e_i \tag{14}
$$

$$
v_i^{(n+1)} = \hat{v_i}+\Delta t\cdot\{-f_t\} \tag{15}
$$

Where $\tilde{v}$ means temporally velocity, and superscript (n) indicates a time step. $\hat{v_i}$ is a temporally velocity without considering the movement of the computational grid. Because the free surface deforms, the computational grid must be restructured. Therefore, it is important that the influence of the computational grid movement is considered. Equation (15) is utilized to take account of the computational grid movement.

Equation (15) is considering in two dimensional coordinate for the simplicity.
Jacobian matrix in two dimension can be described as

$$\begin{bmatrix} \frac{\partial}{\partial t} \\ \frac{\partial}{\partial r} \\ \frac{\partial}{\partial z} \end{bmatrix} = \begin{bmatrix} 1 & \xi_t & \eta_t \\ 0 & \xi_r & \eta_r \\ 0 & \xi_z & \eta_z \end{bmatrix} \begin{bmatrix} \frac{\partial}{\partial \tau} \\ \frac{\partial}{\partial \xi} \\ \frac{\partial}{\partial \eta} \end{bmatrix} \tag{16}$$

$$\begin{bmatrix} \frac{\partial}{\partial \tau} \\ \frac{\partial}{\partial \xi} \\ \frac{\partial}{\partial \eta} \end{bmatrix} = \begin{bmatrix} 1 & r_\tau & z_\tau \\ 0 & r_\xi & z_\xi \\ 0 & r_\eta & z_\eta \end{bmatrix} \begin{bmatrix} \frac{\partial}{\partial t} \\ \frac{\partial}{\partial r} \\ \frac{\partial}{\partial z} \end{bmatrix} \tag{17}$$

Equation (17) is inversely transformed as follows,

$$\begin{bmatrix} \frac{\partial}{\partial t} \\ \frac{\partial}{\partial r} \\ \frac{\partial}{\partial z} \end{bmatrix} = \frac{1}{J} \begin{bmatrix} (r_\xi z_\eta - z_\xi r_\eta) & (-r_\tau z_\eta + z_\tau r_\eta) & (r_\tau z_\xi - r_\tau z_\xi) \\ 0 & z_\eta & -z_\xi \\ 0 & -r_\eta & r_\xi \end{bmatrix} \begin{bmatrix} \frac{\partial}{\partial \tau} \\ \frac{\partial}{\partial \xi} \\ \frac{\partial}{\partial \eta} \end{bmatrix} \tag{18}$$

From Eqs. (16) and (18), the relation of each components are given by

$$\begin{cases} J = r_\xi z_\eta - z_\xi r_\eta \\ \xi_r = \frac{z_\eta}{J}, \qquad \eta_r = -\frac{z_\xi}{J} \\ \xi_z = -\frac{r_\eta}{J}, \qquad \eta_z = \frac{r_\xi}{J} \end{cases} \tag{19}$$

Then equation (15) becomes equation (20) and is further transformed to equation (21).

$$v_i^{(n+1)} = \hat{v}_i - \Delta t \left[\xi_t \frac{\partial \hat{v}_i}{\partial \xi} + \eta_t \frac{\partial \hat{v}_i}{\partial \eta} \right] \tag{20}$$

$$v_i^{(n+1)} = \hat{v}_i + \Delta t \left\{ \frac{\partial \hat{v}_i}{\partial r} r_t + \frac{\partial \hat{v}_i}{\partial z} z_t \right\} \tag{21}$$

Where $\hat{v}_i$ is the velocity in the previous computational grid.
That is, if the computational grid moves $\frac{\partial r}{\partial t}\Delta t$, the velocity in the restructured grid is indicated by equation (21) (See Figure. 2).
This approach can be adapted in the three dimension as well.

The pressure in the equation (14) is solved by the pressure poisson equation. The pressure poisson equation is derived from the continuity equation and equation (14).
[Pressure poisson equation]

$$\nabla^2 P = \frac{\nabla \cdot v_i}{\triangle t} \tag{22}$$

Equation (22) is expanded as follows.

$$\frac{\partial}{\partial \xi}(Jr\xi_r\xi_r\frac{\partial P}{\partial \xi}) + \frac{\partial}{\partial \xi}(Jr\xi_r\zeta_r\frac{\partial P}{\partial \zeta}) + \frac{\partial}{\partial \xi}(Jr\xi_r\eta_r\frac{\partial P}{\partial \eta})$$

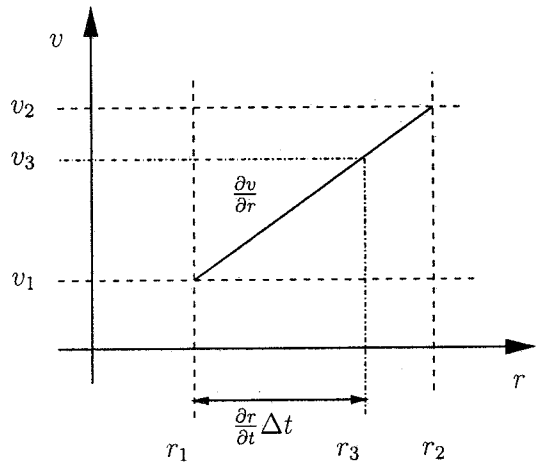

Figure 2: The relation between the velocity and the computational grid

$$
\begin{aligned}
&+ \frac{\partial}{\partial\zeta}(Jr\zeta_r\xi_r\frac{\partial P}{\partial\xi}) + \frac{\partial}{\partial\zeta}(Jr\zeta_r\zeta_r\frac{\partial P}{\partial\zeta}) + \frac{\partial}{\partial\zeta}(Jr\zeta_r\eta_r\frac{\partial P}{\partial\eta}) \\
&+ \frac{\partial}{\partial\eta}(Jr\eta_r\xi_r\frac{\partial P}{\partial\xi}) + \frac{\partial}{\partial\eta}(Jr\eta_r\zeta_r\frac{\partial P}{\partial\zeta}) + \frac{\partial}{\partial\eta}(Jr\eta_r\eta_r\frac{\partial P}{\partial\eta}) \\
&+ \frac{\partial}{\partial\xi}(J\frac{1}{r}\xi_\theta\xi_\theta\frac{\partial P}{\partial\xi}) + \frac{\partial}{\partial\xi}(J\frac{1}{r}\xi_\theta\zeta_\theta\frac{\partial P}{\partial\zeta}) + \frac{\partial}{\partial\xi}(J\frac{1}{r}\xi_\theta\eta_\theta\frac{\partial P}{\partial\eta}) \\
&+ \frac{\partial}{\partial\zeta}(J\frac{1}{r}\zeta_\theta\xi_\theta\frac{\partial P}{\partial\xi}) + \frac{\partial}{\partial\zeta}(J\frac{1}{r}\zeta_\theta\zeta_\theta\frac{\partial P}{\partial\zeta}) + \frac{\partial}{\partial\zeta}(J\frac{1}{r}\zeta_\theta\eta_\theta\frac{\partial P}{\partial\eta}) \\
&+ \frac{\partial}{\partial\eta}(J\frac{1}{r}\eta_\theta\xi_\theta\frac{\partial P}{\partial\xi}) + \frac{\partial}{\partial\eta}(J\frac{1}{r}\eta_\theta\zeta_\theta\frac{\partial P}{\partial\zeta}) + \frac{\partial}{\partial\eta}(J\frac{1}{r}\eta_\theta\eta_\theta\frac{\partial P}{\partial\eta}) \\
&+ \frac{\partial}{\partial\xi}(Jr\xi_z\xi_z\frac{\partial P}{\partial\xi}) + \frac{\partial}{\partial\xi}(Jr\xi_z\zeta_z\frac{\partial P}{\partial\zeta}) + \frac{\partial}{\partial\xi}(Jr\xi_z\eta_z\frac{\partial P}{\partial\eta}) \\
&+ \frac{\partial}{\partial\zeta}(Jr\zeta_z\xi_z\frac{\partial P}{\partial\xi}) + \frac{\partial}{\partial\zeta}(Jr\zeta_z\zeta_z\frac{\partial P}{\partial\zeta}) + \frac{\partial}{\partial\zeta}(Jr\zeta_z\eta_z\frac{\partial P}{\partial\eta}) \\
&+ \frac{\partial}{\partial\eta}(Jr\eta_z\xi_z\frac{\partial P}{\partial\xi}) + \frac{\partial}{\partial\eta}(Jr\eta_z\zeta_z\frac{\partial P}{\partial\zeta}) + \frac{\partial}{\partial\eta}(Jr\eta_z\eta_z\frac{\partial P}{\partial\eta}) \\
&= \frac{1}{\Delta t}\Big[\frac{\partial}{\partial\xi}(Jr\tilde{V_\xi}) + \frac{\partial}{\partial\zeta}(Jr\tilde{V_\zeta}) + \frac{\partial}{\partial\eta}(Jr\tilde{V_\eta})\Big] \qquad (23)
\end{aligned}
$$

Where $\tilde{V_\xi}$,$\tilde{V_\zeta}$ and $\tilde{V_\eta}$ are defined by

$$
\begin{aligned}
\tilde{V_\xi} &= \xi_r\tilde{v_r} + \frac{1}{r}\xi_\theta\tilde{v_\theta} + \xi_z\tilde{v_z} \\
\tilde{V_\zeta} &= \zeta_r\tilde{v_r} + \frac{1}{r}\zeta_\theta\tilde{v_\theta} + \zeta_z\tilde{v_z} \\
\tilde{V_\eta} &= \eta_r\tilde{v_r} + \frac{1}{r}\eta_\theta\tilde{v_\theta} + \eta_z\tilde{v_z}\,,
\end{aligned}
$$

which are called as **contravariant temporally velocities**.
To solve the pressure variation implicitly, equation (23) is calculated by successive over relaxation method (SOR method) in this analysis.

2.3 Boundary condition

2.3.1 Boundary condition of the velocity

To derive the boundary condition of the velocity at the free surface, the balance between the shearing stress and the surface tension must be considered.
The relation between the shearing stress and the surface tension is shown in figure 3.

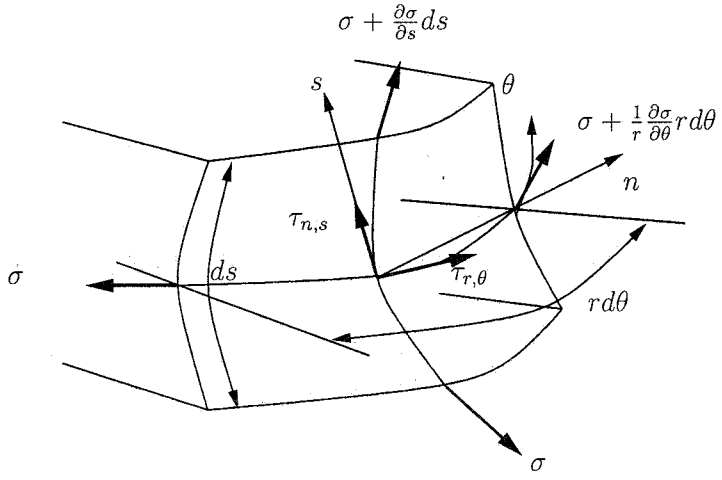

Figure 3: The stress balance between the shearing stress and the surface tension

From figure 3, the equations of the balance between shearing stress and the surface tension are described as

$$\begin{cases} \tau_{n,s} \cdot r d\theta ds = \{(\sigma + \frac{\partial \sigma}{\partial s} \cdot ds) - \sigma\} \cdot r d\theta \\ \tau_{r,\theta} \cdot r d\theta ds = \{(\sigma + \frac{1}{r}\frac{\partial \sigma}{\partial \theta} \cdot r d\theta) - \sigma\} \cdot ds \end{cases} \tag{24}$$

Newton's law of viscosity equation is expressed as follows.

$$\begin{cases} \tau_{n,s} = \mu\{\frac{\partial v_s}{\partial n} + \frac{\partial v_n}{\partial s}\} \\ \tau_{r,\theta} = \mu\{\frac{1}{r}\frac{\partial v_r}{\partial \theta} + r\frac{\partial}{\partial r}(\frac{v_\theta}{r})\} \end{cases} \tag{25}$$

From Eqs. (24) and (25) equation (26) is derived.

$$\begin{cases} \mu\{\frac{\partial v_s}{\partial n} + \frac{\partial v_n}{\partial s}\} = \frac{\partial \sigma}{\partial s} \\ \mu\{\frac{1}{r}\frac{\partial v_r}{\partial \theta} + r\frac{\partial}{\partial r}(\frac{v_\theta}{r})\} = \frac{1}{r}\frac{\partial \sigma}{\partial \theta} \end{cases} \tag{26}$$

If the velocity upon the free surface in the normal direction is assumed to be zero, equation (26) can be shown as follows.

$$\begin{cases} \mu\frac{\partial v_s}{\partial n} = \frac{\partial \sigma}{\partial s} \\ \mu\{\frac{1}{r}\frac{\partial v_r}{\partial \theta} + r\frac{\partial}{\partial r}(\frac{v_\theta}{r})\} = \frac{1}{r}\frac{\partial \sigma}{\partial \theta} \end{cases} \tag{27}$$

Equation (27) can be non-dimensionalized as following equations.

$$\begin{cases} \frac{\partial v_s}{\partial n} = -\frac{\partial T}{\partial s} \\ \frac{1}{r}\frac{\partial v_r}{\partial \theta} + r\frac{\partial}{\partial r}(\frac{v_\theta}{r}) = -\frac{1}{r}\frac{\partial T}{\partial \theta} \end{cases} \tag{28}$$

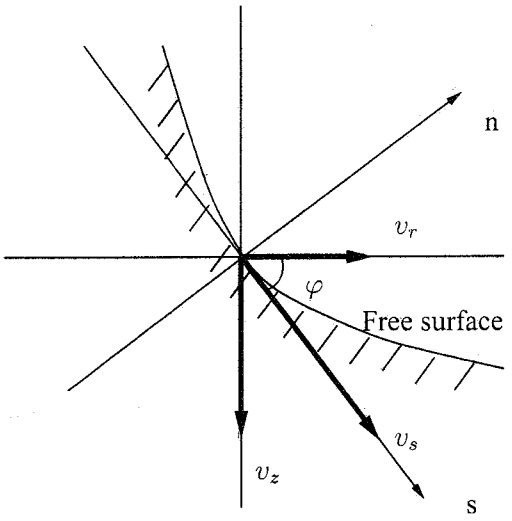

$$\begin{cases} v_r = v_s \cos\varphi \\ v_z = v_s \sin\varphi \end{cases} \tag{29}$$

$$\Longleftrightarrow \begin{cases} v_s = \frac{v_r}{\cos\varphi} \\ v_s = \frac{v_z}{\sin\varphi} \end{cases} \tag{30}$$

$$\Longleftrightarrow \begin{cases} \frac{\partial v_s}{\partial n} = \frac{\partial}{\partial n}\left(\frac{v_r}{\cos\varphi}\right) \\ \frac{\partial v_s}{\partial n} = \frac{\partial}{\partial n}\left(\frac{v_z}{\sin\varphi}\right) \end{cases} \tag{31}$$

$$\Longleftrightarrow \begin{cases} \frac{\partial v_r}{\partial n} = -\cos\varphi \frac{\partial T}{\partial s} \\ \frac{\partial v_z}{\partial n} = -\sin\varphi \frac{\partial T}{\partial s} \end{cases} \tag{32}$$

Figure 4: The velocity at the free surface

In the equation of the relation between normal and tangential directions, the tangential velocity v_s is divided into radius and axial directions (See figure. 4).
Generally the following relations are derived in the normal and tangential directions.
[Normal derivatives]

$$\frac{\partial \phi}{\partial n^{(\xi)}} = \frac{1}{J\sqrt{\alpha}}(\alpha\phi_\xi - \beta\phi_\eta) \tag{33}$$

$$\frac{\partial \phi}{\partial n^{(\eta)}} = \frac{1}{J\sqrt{\gamma}}(-\beta\phi_\xi + \gamma\phi_\eta) \tag{34}$$

[Tangential derivatives]

$$\frac{\partial \phi}{\partial s^{(\xi)}} = \frac{1}{\sqrt{\alpha}}\phi_\eta \tag{35}$$

$$\frac{\partial \phi}{\partial s^{(\eta)}} = \frac{1}{\sqrt{\gamma}}\phi_\xi \tag{36}$$

Here $\alpha = r_\eta^2 + z_\eta^2$, $\beta = r_\xi r_\eta + z_\xi z_\eta$, $\gamma = r_\xi^2 + z_\xi^2$.
Using equation (33), the equation of the stress balance between normal and tangential directions is obtained.

$$\frac{1}{J\sqrt{\alpha}}\left(\alpha\frac{\partial v_z}{\partial \xi} - \beta\frac{\partial v_z}{\partial \eta}\right) = -\sin\varphi\frac{1}{\sqrt{\alpha}}\frac{\partial T}{\partial \eta} \tag{37}$$

The axial velocity v_z is derived from equation (37). And the radius velocity is derived from the relation of following equation.

$$v_r = \frac{\cos\varphi}{\sin\varphi}v_z \tag{38}$$

On the other hand, the boundary condition of the circumferential velocity is defined by

$$\frac{1}{r}\frac{\partial v_r}{\partial \theta} + r\frac{\partial}{\partial r}\left(\frac{v_\theta}{r}\right) = -\frac{1}{r}\frac{\partial T}{\partial \theta} \tag{39}$$

Equation (39) is transformed to the computational domain by the Jacobian matrix as

$$\begin{aligned} & \frac{1}{r}\left\{\xi_\theta\frac{\partial v_r}{\partial \xi}+\zeta_\theta\frac{\partial v_r}{\partial \zeta}+\eta_\theta\frac{\partial v_r}{\partial \eta}\right\}+r\left\{\xi_r\frac{\partial}{\partial \xi}(\frac{v_\theta}{r})+\zeta_r\frac{\partial}{\partial \zeta}(\frac{v_\theta}{r})+\eta_r\frac{\partial}{\partial \eta}(\frac{v_\theta}{r})\right\} \\ = & -\frac{1}{r}\left\{\xi_\theta\frac{\partial T}{\partial \xi}+\zeta_\theta\frac{\partial T}{\partial \zeta}+\eta_\theta\frac{\partial T}{\partial \eta}\right\} . \end{aligned} \tag{40}$$

2.3.2 Boundary condition of the temperature

The condition of the heat transfer over the free surface is assumed to be adiabatic. Therefore the equation of the boundary condition of the temperature is

$$\frac{\partial T}{\partial n}=0 \tag{41}$$

Equation (41) is transformed by the Jacobian matrix as

$$\frac{\partial T}{\partial \xi}\frac{\partial \xi}{\partial n}+\frac{\partial T}{\partial \zeta}\frac{\partial \zeta}{\partial n}+\frac{\partial T}{\partial \eta}\frac{\partial \eta}{\partial n}=0 . \tag{42}$$

To transform into the computational domain, equation (33) is utilized.

$$\frac{\partial T}{\partial n}=\frac{1}{J\sqrt{\alpha}}(\alpha\frac{\partial T}{\partial \xi}-\beta\frac{\partial T}{\partial \eta})=0 \tag{43}$$

2.3.3 The treatment of the liquid center axis

In this analysis the governing equations are described in the cylindrical coordinate. Therefore the center of the cylinder ($r=0$) can not be solved directly by the present equations (Eqs.(2)-(3)). This problem is solved through by the method below. The computational grid is fixed at the center. [Navier-Stokes equation of the liquid center (axial direction)]

$$\begin{aligned} & r\frac{\partial v_z}{\partial t}+\frac{\partial}{\partial r}(rv_rv_z)+\frac{\partial}{\partial \theta}(v_\theta v_z)+\frac{\partial}{\partial z}(rv_z^2) \\ = & -r\frac{\partial P}{\partial z}+\frac{Pr}{Ma}\left[\frac{\partial}{\partial r}(r\frac{\partial v_z}{\partial r})+\frac{\partial}{\partial \theta}(\frac{1}{r}\frac{\partial v_z}{\partial \theta})+\frac{\partial}{\partial z}(r\frac{\partial v_z}{\partial z})\right]+rT\frac{Gr}{Re^2} \end{aligned} \tag{44}$$

Equation (44) is integrated in all directions.

$$\begin{aligned} & \frac{\partial v_z}{\partial t}+\frac{\Delta\theta}{\pi\Delta r}\sum_{\theta=0}^{2\pi}(v_rv_z)+\frac{1}{\Delta z}\left[v_z^2\right]_0^{\Delta z} \\ = & -\frac{\partial P}{\partial z}+\frac{Pr}{Ma}\left[\frac{\Delta\theta}{\pi\Delta r}\sum_{\theta=0}^{2\pi}\frac{\partial v_z}{\partial r}\Big|_{\Delta r}+\frac{1}{\Delta z}\left[\frac{\partial v_z}{\partial z}\right]_0^{\Delta z}\right]+\frac{Gr}{Re^2}T \end{aligned} \tag{45}$$

As for the radius and circumference velocity in the center, the velocity is summed over the surrounding mesh points (See figure 5).

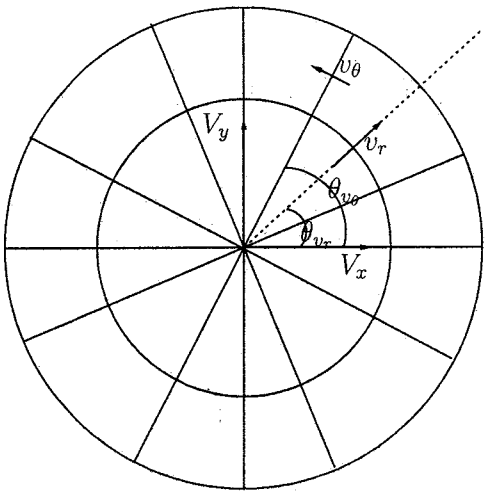

$$V_x = \sum_{j=0}^{2\pi} \left\{ v_r \cos\theta_{v_r} + v_\theta \cos(\theta_{v_\theta} + \frac{\pi}{2}) \right\} \quad (46)$$

$$V_y = \sum_{j=0}^{2\pi} \left\{ v_r \sin\theta_{v_r} + v_\theta \sin(\theta_{v_\theta} + \frac{\pi}{2}) \right\} \quad (47)$$

Figure 5: The velocity at the center axis

After the summation, the velocities V_x, V_y are divided into the radius and circumference components (v_r, v_θ).

$$v_r = \left[V_x \cos\theta_{v_r} + V_y \cos(\frac{\pi}{2} - \theta_{v_r}) \right] \frac{1}{nj} \quad (48)$$

$$v_\theta = \left[V_x(-\sin\theta_{v_\theta}) + V_y \sin(\frac{\pi}{2} - \theta_{v_\theta}) \right] \frac{1}{nj} \quad (49)$$

Here nj shows the division number of the circumference direction. Such treatment at the center axis is also applied to the energy equation.
[Energy equation of the liquid center]

$$r\frac{\partial T}{\partial t} + \frac{\partial}{\partial r}(rv_rT) + \frac{\partial}{\partial \theta}(v_\theta T) + \frac{\partial}{\partial z}(rv_zT) = \frac{1}{Ma}\left[\frac{\partial}{\partial r}(r\frac{\partial T}{\partial r}) + \frac{\partial}{\partial \theta}(\frac{1}{r}\frac{\partial T}{\partial \theta}) + \frac{\partial}{\partial z}(r\frac{\partial T}{\partial z}) \right] \quad (50)$$

Equation (50) is integrated in all directions.

$$\frac{\partial T}{\partial t} + \frac{\Delta\theta}{\pi\Delta r}\sum_{\theta=0}^{2\pi}(v_rT) + \frac{1}{\Delta z}\left[v_zT\right]_0^{\Delta z} = \frac{1}{Ma}\left\{ \frac{\Delta\theta}{\pi\Delta r}\sum_{\theta=0}^{2\pi}\frac{\partial T}{\partial r}\Big|_{\Delta r} + \frac{1}{\Delta z}\left[\frac{\partial T}{\partial z}\right]_0^{\Delta z} \right\} \quad (51)$$

Also the pressure Poisson equation has to be solved at the liquid center axis.
The pressure Poisson equation is derived from Eqs. (52) and (53).

$$\left[\frac{2}{\Delta z^2} + \frac{4}{3\Delta r^2}\right] P_C - \left[\frac{1}{\Delta z^2}(P_N + P_S) + \frac{1}{nj}\frac{4}{3\Delta r^2}\sum_{j=0}^{nj} P_j\right]$$

$$= \left[-\frac{1}{\Delta z}(\tilde{v}_{z_N} - \tilde{v}_{z_S}) - \frac{2}{nj\Delta r}\sum_{j=0}^{nj}\tilde{v}_{r_j}\right]\frac{1}{\Delta t} \quad (54)$$

2.4 The free surface shape

To computate the free surface shape, the stress balance over the free surface must be considered. Along the free surface between two immiscible fluids (1) and (2) the forces on adjacent surface

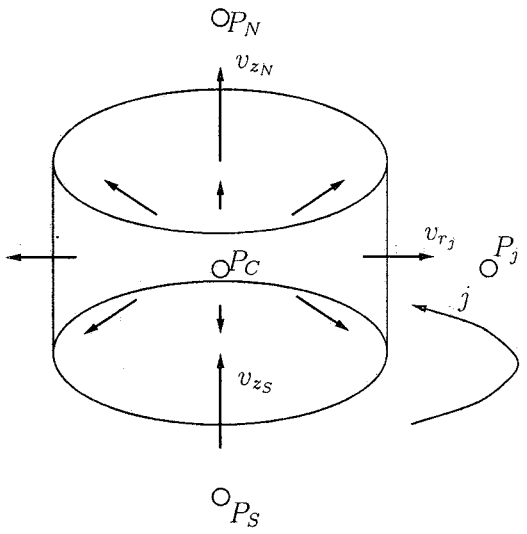

Figure 6: The model of the in and outflows

From the figure 6 the continuity equation is defined as

$$\pi\Delta r^2(v_{z_N} - v_{z_S}) + \frac{2\pi}{nj}\Delta r\Delta z\sum_{j=0}^{nj} v_{r_j} = 0 \quad (52)$$

Time advancement is described as follows.

$$\begin{cases} v_{z_N}^{(n+1)} = \tilde{v}_{z_N} - \Delta t\frac{P_N - P_C}{\Delta z} \\ v_{z_S}^{(n+1)} = \tilde{v}_{z_S} - \Delta t\frac{P_C - P_S}{\Delta z} \\ v_{r_j}^{(n+1)} = \tilde{v}_{r_j} - \Delta t\frac{P_j - P_C}{\Delta r + \frac{1}{2}\Delta r_j} \end{cases} \quad (53)$$

where, Δr_j is defined as $\Delta r_j = \Delta r$.

element of (1) and (2) must be the same.
If the surface is plane and the surface tension is constant, the stress balance over the free surface leads

$$\mathbf{S}^{(1)} \cdot \mathbf{n} = \mathbf{S}^{(2)} \cdot \mathbf{n}, \quad (55)$$

where $\mathbf{S}$ is the stress tensor.
The each components in the stress tensor are described as

$$S_{ij} = -P\delta_{ij} + \lambda\Theta\delta_{ij} + \mu e_{ij}, \quad (56)$$

where λ and μ are **coefficient of viscosity** and **second coefficient of viscosity**, respectively.
In this analysis it is assumed that the fluid is Newtonian, so that

$$\Theta = div\nu = 0. \quad (57)$$

In addition, if the free surface has curvature and the surface tension varies along the interface, the equation of the stress balance is described as [5]

$$\mathbf{S}^{(1)} \cdot \mathbf{n} + \sigma(\nabla \cdot \mathbf{n})\mathbf{n} - (\mathbf{I} - \mathbf{nn}) \cdot \nabla\sigma = \mathbf{S}^{(2)} \cdot \mathbf{n}, \quad (58)$$

where $\mathbf{I}$ is the identity matrix, and $\mathbf{n}$ is the unit normal vector directed out of liquid (1) into the ambient fluid (2).
The element $\sigma(\nabla \cdot \mathbf{n})$ in the second term is the Laplace pressure. The mean curvature of the interface,

$$\nabla \cdot \mathbf{n} = \frac{1}{R_1} + \frac{1}{R_2}, \quad (59)$$

can be expressed as the sum of the inverse principle radii of curvature R_1 and R_2. The second term in equation (58) indicates the surface force acting tangentially originated from the surface tension σ. The operator $\mathbf{I} - \mathbf{nn}$ represents the orthogonal projection of a vector onto the tangent plane

defined by $\mathbf{n}$.
Besides the influence of the surface shape and the surface tension, the action of the gravity is taken account into the equation of the stress balance,

$$\mathbf{S}^{(1)} \cdot \mathbf{n} + \sigma(\nabla \cdot \mathbf{n})\mathbf{n} - (\mathbf{I} - \mathbf{nn}) \cdot \nabla\sigma + \rho^{(1)} g(H - z)\mathbf{n} = \mathbf{S}^{(2)} \cdot \mathbf{n} + \rho^{(2)} g(H - z)\mathbf{n} \tag{60}$$

Equation (60) is described in non-dimensional manner.

$$\mathbf{S}^{(1)} \cdot \mathbf{n} + \left(\frac{1}{Ca} - T^*\right)(\nabla \cdot \mathbf{n})\mathbf{n} + (\mathbf{I} - \mathbf{nn}) \cdot \nabla T^* = \mathbf{S}^{(2)} - \frac{Bo}{Ca}(H - z)\mathbf{n} \tag{61}$$

The scales used for non-dimensionalization were indicated in table 1. In addition, the normalized temperature $T^* = (T - T_0)/\Delta T$ has been introduced.
The surface tension is non-dimensionalized by using the normalized temperature,

$$\sigma(T) = \sigma_0(T_0) - \sigma_T(T - T_0) \tag{62}$$

$$\Longleftrightarrow \frac{\sigma}{\sigma_T \Delta T} = \frac{\sigma_0(T_0)}{\sigma_T \Delta T} - T^* \tag{63}$$

$$\Longleftrightarrow \sigma^* = \frac{1}{Ca} - T^*, \tag{64}$$

where $\sigma^* = \frac{\sigma}{\sigma_T \Delta T}$ and the capillary number is defined by

$$Ca = \frac{\sigma_T \Delta T}{\sigma_0(T_0)}. \tag{65}$$

From equation (64), the gradient of the surface tension is expressed by the normalized temperature,

$$\nabla\sigma^* = -\nabla T^*. \tag{66}$$

Bo is called as **Bond number** which is defined by

$$Bo = \frac{(\rho^{(1)} - \rho^{(2)})gH^2}{\sigma_0} \tag{67}$$

The asterisk is omitted hereafter.
Equation (61) is expanded as follows.
Using the unit normal vector

$$\mathbf{n} = \frac{1}{N}\left(\mathbf{e}_r - \frac{1}{R}\frac{\partial R}{\partial \theta}\mathbf{e}_\theta - \frac{\partial R}{\partial z}\mathbf{e}_z\right) \tag{68}$$

with the normalizing denominator

$$N = \left[1 + \left(\frac{\partial R}{\partial z}\right)^2 + \frac{1}{R^2}\left(\frac{\partial R}{\partial \theta}\right)^2\right]^{\frac{1}{2}}, \tag{69}$$

the surface curvature can be expressed as

$$\begin{aligned}\nabla \cdot \mathbf{n} = \frac{-1}{R^3 N^3}\Bigg[& R\frac{\partial^2 R}{\partial z^2}\left\{R^2 + \left(\frac{\partial R}{\partial \theta}\right)^2\right\} \\ & + 2\frac{\partial R}{\partial z}\frac{\partial R}{\partial \theta}\left(\frac{\partial R}{\partial z}\frac{\partial R}{\partial \theta} - R\frac{\partial^2 R}{\partial z \partial \theta}\right) \\ & - \left\{1 + \left(\frac{\partial R}{\partial z}\right)^2\right\}\left\{R^2 + 2\left(\frac{\partial R}{\partial \theta}\right)^2 - R\frac{\partial^2 R}{\partial \theta^2}\right\}\Bigg]\end{aligned} \tag{70}$$

The stress tensor is indicated as

$$S_{ij} = -P\delta_{ij} + \mu e_{ij}\,, \tag{71}$$

where e_{ij} in the cylindrical coordinate is defined by

$$e_{rr} = \frac{\partial v_r}{\partial r},\quad e_{\theta\theta} = \frac{1}{r}\frac{\partial v_\theta}{\partial \theta} + \frac{v_r}{r},\quad e_{zz} = \frac{\partial v_z}{\partial z},$$
$$e_{r\theta} = \frac{1}{2}\left\{ r\frac{\partial}{\partial r}\left(\frac{v_\theta}{r}\right) + \frac{1}{r}\frac{\partial v_r}{\partial \theta}\right\},\quad e_{\theta z} = \frac{1}{2}\left\{\frac{1}{r}\frac{\partial v_z}{\partial \theta} + \frac{\partial v_\theta}{\partial z}\right\},\quad e_{zr} = \frac{1}{2}\left\{\frac{\partial v_r}{\partial z} + \frac{\partial v_z}{\partial r}\right\} \tag{72}$$

The unit normal vector and the identity matrix are shown below.

$$\mathbf{n} = \begin{bmatrix} n_r \\ n_\theta \\ n_z \end{bmatrix} \tag{73}$$

$$\mathbf{I} = \begin{bmatrix} 1 & 0 & 0 \\ 0 & 1 & 0 \\ 0 & 0 & 1 \end{bmatrix} \tag{74}$$

nn represents the dyadic product which is expressed as

$$\mathbf{I} = \begin{bmatrix} n_r \\ n_\theta \\ n_z \end{bmatrix}\begin{bmatrix} n_r \\ n_\theta \\ n_z \end{bmatrix} = \begin{bmatrix} n_r^2 & n_r n_\theta & n_r n_z \\ n_\theta n_r & n_\theta^2 & n_\theta n_z \\ n_z n_r & n_z n_\theta & n_z^2 \end{bmatrix} \tag{75}$$

The components of the surface tension gradient is

$$\nabla\sigma = \begin{bmatrix} \frac{\partial\sigma}{\partial r} \\ \frac{1}{r}\frac{\partial\sigma}{\partial\theta} \\ \frac{\partial\sigma}{\partial z} \end{bmatrix} \tag{76}$$

From these matrices, the equation of the stress balance is led in the three directions.
Since the two directions of the curvature exist in the three dimension, the two tri-diagonal matrices must be considered for axial and circumferential directions. The tridiagonal equations are indicated below.
(Radius direction)

$$\frac{\partial^2 R}{\partial z^2} = \frac{-R^3 N^3}{R\{R^2 + (\partial R/\partial\theta)^2\}(1/Ca - T)} \left[Re(P^{(1)} - P^{(2)}) \right.$$
$$-\frac{Bo}{Ca}(H - z)$$
$$-\frac{\partial v_r}{\partial r}$$
$$-\frac{1}{2}\{r\frac{\partial}{\partial r}(\frac{v_\theta}{r}) + \frac{1}{r}\frac{\partial v_r}{\partial\theta}\}\frac{n_\theta}{n_r} - \frac{1}{2}\{\frac{\partial v_r}{\partial z} + \frac{\partial v_z}{\partial r}\}\frac{n_z}{n_r}$$
$$\left. -\frac{1 - n_r^2}{n_r}\frac{\partial T}{\partial r} + n_\theta\frac{1}{r}\frac{\partial T}{\partial\theta} + n_z\frac{\partial T}{\partial z}\right]$$
$$+\frac{1}{R\{R^2 + (\partial R/\partial\theta)^2}\left[-2\frac{\partial R}{\partial z}\frac{\partial R}{\partial\theta}(\frac{\partial R}{\partial z}\frac{\partial R}{\partial\theta} - R\frac{\partial^2 R}{\partial z\partial\theta})\right.$$
$$\left. +\{1 + (\frac{\partial R}{\partial z})^2\}\{R^2 + 2(\frac{\partial R}{\partial\theta})^2 - R\frac{\partial^2 R}{\partial\theta^2}\}\right] \tag{77}$$

(Circumferential direction)

$$
\begin{aligned}
\frac{\partial^2 R}{\partial \theta^2} = \frac{-R^3 N^3}{R\{1+(\partial R/\partial z)^2\}(1/Ca - T)} & \Big[Re(P^{(1)} - P^{(2)}) \\
& -\frac{Bo}{Ca}(H-z) \\
& -\frac{\partial v_r}{\partial r} \\
& -\frac{1}{2}\{r\frac{\partial}{\partial r}(\frac{v_\theta}{r}) + \frac{1}{r}\frac{\partial v_r}{\partial \theta}\}\frac{n_\theta}{n_r} - \frac{1}{2}\{\frac{\partial v_r}{\partial z} + \frac{\partial v_z}{\partial r}\}\frac{n_z}{n_r} \\
& -\frac{1-n_r^2}{n_r}\frac{\partial T}{\partial r} + n_\theta \frac{1}{r}\frac{\partial T}{\partial \theta} + n_z \frac{\partial T}{\partial z} \Big] \\
& + \frac{1}{R\{1+(\partial R/\partial z)^2\}} \Big[-R\frac{\partial^2 R}{\partial z^2}\{R^2 + (\frac{\partial R}{\partial \theta})^2\} \\
& -2\frac{\partial R}{\partial z}\frac{\partial R}{\partial \theta}(\frac{\partial R}{\partial z}\frac{\partial R}{\partial \theta} - R\frac{\partial^2 R}{\partial z \partial \theta}) \Big] \\
& + \frac{2}{R}(\frac{\partial R}{\partial \theta})^2 + R
\end{aligned}
\tag{78}
$$

In addition to the these tridiagonal equations, the constant volume equation has to be solved to maintain the volume of the liquid bridge.

$$
\int_0^H \int_0^{2\pi} \frac{1}{2} R^2 d\theta dz = V \tag{79}
$$

The position of the free surface ,R, is solved by using Tri-Diagonal Matrix Algorithm (TDMA) derived from Eqs. (61) and (79). The tri-diagonal matrices are given below.
(Axial direction)

$$
\begin{bmatrix}
a^H_{1,0}\; c^H_{1,0} & & & & & & d^H_{1,0} \\
b^H_{1,1}\; a^H_{1,1}\; c^H_{1,1} & & & & & & d^H_{1,1} \\
\ddots & & & & & & \vdots \\
 & b^H_{1,nk}\; a^H_{1,nk}\; c^H_{1,nk} & & & & & d^H_{1,nk} \\
 & b^H_{1,nk+1}\; a^H_{1,nk+1} & & & & & d^H_{1,nk+1} \\
 & & \ddots & & & & \vdots \\
 & & a^H_{nj,0}\; c^H_{nj,0} & & & & d^H_{nj,0} \\
 & & b^H_{nj,1}\; a^H_{nj,1}\; c^H_{nj,1} & & & & d^H_{nj,1} \\
 & & & \ddots & & & \vdots \\
 & & & & b^H_{nj,nk}\; a^H_{nj,nk}\; c^H_{nj,nk} & & d^H_{nj,nk} \\
 & & & & b^H_{nj,nk+1}\; a^H_{nj,nk+1} & & d^H_{nj,nk+1} \\
e^H_{1,0}\, e^H_{1,1}\, e^H_{1,2} \cdots e^H_{1,nk-1}\, e^H_{1,nk} & e^H_{1,nk+1} \cdots e^H_{nj,0}\, e^H_{nj,1}\, e^H_{nj,2} \cdots e^H_{nj,nk-1} & e^H_{nj,nk} & e^H_{nj,nk+1} & & & G^H
\end{bmatrix}
\begin{bmatrix}
R_{1,0} \\ R_{1,1} \\ \vdots \\ R_{1,nk} \\ R_{1,nk+1} \\ \vdots \\ R_{nj,0} \\ R_{nj,1} \\ \vdots \\ R_{nj,nk} \\ R_{nj,nk+1} \\ P_s
\end{bmatrix}
=
\begin{bmatrix}
f^H_{1,0} \\ f^H_{1,1} \\ \vdots \\ f^H_{1,nk} \\ f^H_{1,nk+1} \\ \vdots \\ f^H_{nj,0} \\ f^H_{nj,1} \\ \vdots \\ f^H_{nj,nk} \\ f^H_{nj,nk+1} \\ Q^H
\end{bmatrix}
\tag{80}
$$

The last array in this matrix gives the constant volume condition.
(Circumferential direction; for each R_k)

$$\begin{bmatrix} b^C_{1,k} & c^C_{1,k} & & & a^C_{1\,k} \\ a^C_{2,k} & b^C_{2,k} & c^C_{2,k} & & \\ & \ddots & & & \\ & & a^C_{nj-1,k} & b^C_{nj-1\,k} & c^C_{nj-1,k} \\ c^C_{nj\,k} & & & a^C_{nj,k} & b^C_{nj,k} \end{bmatrix} \begin{bmatrix} R_{1,k} \\ R_{2\,k} \\ \vdots \\ R_{nj-1\,k} \\ R_{nj,k} \end{bmatrix} = \begin{bmatrix} d^C_{1,k} \\ d^C_{2\,k} \\ \vdots \\ d^C_{nj-1,k} \\ d^C_{nj,k} \end{bmatrix} \tag{81}$$

The free surface shape is derived from these matrices.

3 RESULTS AND DISCUSSION

3.1 Flow near a corner in 2-dimensional axisymmetric simulations

3.1.1 Flow near a corner

For high Pr fluid, the isotherm is compressed and the velocity on the free surface exhibits a peak near a corner. Thus the fine mesh is needed to resolve the distributions near the corner.

In the vicinity of the corner, the flow velocity is very small, one can assume

$$\mathbf{U} \cdot \nabla \mathbf{U} \ll \nu \nabla^2 \mathbf{U} \tag{82}$$

Accordingly, the Navier-Stokes equation can be simplified field as

$$\nu \nabla^2 \mathbf{U} = 0 \tag{83}$$

The solution of equation (83) has been obtained by Kuhlmann [6]. When a contact angle between the free surface and the endwall is $\pi/2$, the axial velocity on the free surface is obtained by following relation.

$$U_z = -\frac{2}{\pi}\omega_0, \tag{84}$$

where U_z is the axial velocity on the free surface, and ω_0 is the vorticity which is determained by the temperaure gradient on the free surface.
Accordingly, the velocity on the free surface can be related to the temperature gradient as

$$U_z = -\frac{2}{\pi}\frac{\partial T}{\partial z} \tag{85}$$

This equation (85) gives the surface velocity near a corner.

3.1.2 Influence of the spacing

On the free surface near the corner, the influence of spacing on the distributions of velocity and temperature are examined. The influence is investigated for the conditions given Tables 2 and 3.

Table 2: The number of grid points

$R \times Z$	40×40	60×60	100×100	400×400	400×800

Table 3: The computational conditions

Ma	Pr	Bi	Gr	Ar
10000	28	0	0	0.5

Figures 8 and 9 are the distributions of the axial velocity and the temperature on the free surface. It is found that the distributions of velocity and temperature in the neighborhood on the free surface at mid-height are hardly influenced by the spacing for grid points 40×40 and 400×800. For high Pr, the distribution of temperature on the free surface is strongly dependent on the magnitude of the surface velocity. Here, the distribution of axial velocity exibits a distinct peak near a corner, because the temperature gradient increases near the corner. Remarkable, the oscillation of the velocity is observed at a cold corner. This indicates that the spacing is not sufficiently fine to resolve the velocity and the temperature gradient at the corner.

Figures 10 and 11 show the distributions of the temperature gradient at cold and hot corners. It is found that the magnitude of the temperature gradient at the endwall increases with increasing grid points, because a large temperature gradient can be attained only when enough fine mesh is employed. The temperature gradient tends to be a constant value at the endwall itself. In the simulation, the distribution of temperature gradient calculated by using the 400×400 grid points agrees with the one by the 400×800.

We will derive the constant temperature gradient near a corner from the energy equation.
Assuming 2-dimensional axisymmetric flow, the following conditions can be applied

$$U_\theta = 0, \ \frac{1}{r^2}\frac{\partial^2 T}{\partial \theta^2} = 0 \tag{86}$$

In the straight cylinder, the radial velocity becomes

$$U_r = 0 \tag{87}$$

On the free surface.
Since the heat conduction in the z direction is dominant, the radial heat conductive term is negligible :

$$\frac{1}{r}\frac{\partial}{\partial r}\left(r\frac{\partial T}{\partial r}\right) = 0 \tag{88}$$

Accordingly, we get the energy equation as follows :

$$U_z\frac{dT}{dz} = \frac{1}{Ma}\frac{d^2T}{dz^2} \tag{89}$$

Integrating equation (89) to z yields

$$\frac{dT}{dz} = ce^{Ma\int U_z dz} \tag{90}$$

where, c is an integration constant.
Here, we expand the velocity on the free surface in terms of z as follows :

$$U_z = -az - bz^2 + \cdots \tag{91}$$

The integrated equation (91) becomes

$$\int U_z dz = -\frac{a}{2}z^2 - \frac{b}{3}z^3 + \cdots \tag{92}$$

As the result, we obtain the temperature gradient as

$$\frac{dT}{dz} = ce^{-Ma\frac{a}{2}z^2}, \tag{93}$$

The temperature gradient for z→0 becomes
Thus,

$$\frac{dT}{dz} = const. \tag{94}$$

Figure 12 shows the distributions of the temperature gradient obtained numerically and analytically. Both distributions agree well near a corner.

Figures 13 and 14 show the distribution of the velocity on the free surface for various grid spacing. The straight line is the exact solution obtained by equation (85). As the number of grid points increases, the peak of velocity at the cold corner approaches to that of the exact solution. At the hot corner, the peak of the velocity approaches to one by the exact solution with increasing mesh number. The value of the peak of the velocity calculated by using the 400×400 grid points agrees with that of the exact solution, that of 400 × 800 also agrees well. Thus, the number of 400×400 grid points is needed at least in this conditions. When the number of the radial grid point is not sufficient, the value of the peak of velocity tends to exceed the value by the exact solution

3.1.3 Influence of Pr and Ma

The influence of Pr and Ma upon the distribution of the temperature gradient and the velocity on the free surface near a corner is investigated.
Calculated conditions are
Ma= 1000, Pr=28
Ma= 2500, Pr=28
Ma=10000, Pr=28,4,67
Ma=40000, Pr=28
Here, Ar, Bi and Gr are 0.5, 0 and 0, respectively.

Figures 15 and 16 show the distribution of the temperature and the velocity on the free surface for various Pr. In case of a constant Ma, it is found that the influence of Pr upon the distributions on the free surface is large around the mid-height and is small near a corner.

Figures 17 and 18 show the distributions of the temperature and the velocity on the free surface. For a high Ma, because the surface velocity is large, the most of the heat on the free surface

is transfered directly to the cold endwall by the surface flow before the heat is conducted to the inside of liquid bridge. Accordingly, as Ma increases, the large surface velocity causes the temperature distribution on the free surface to be flat band around the at mid-height.

Figures 19 and 20 show the distributions of the axial velocity on the free surface near a corners. The distributions of the axial velocity are in agreement with the results obtained by the exact solution. In case of $Ma = 40000$, the value of peak exceeds the exact solution, because the spacing is not fine enough. For higher Ma, the accurate computation requires a large number of grid pints.

Figures 21 and 22 show the distributions of temperature gradients near the hot and the cold corners. The temperature gradients at the hot and the cold endwalls arrive at a constant value, which increase with increasing Ma. The relation between temperature gradient and Ma becomes linear in the logarithmic plot. This relations agree well with the result of the scaling analysis performed by Canright [5].

3.2 Three dimensional simulations

3.2.1 Comparison with the linear stability analysis

The simulations of liquid bridges with statically and dynamically deformed free surface are performed. The results are first compared with the linear stability analysis (LSA). Table 4 shows the conditions for the comparisons with LSA. Here, α is the contact angle between the free surface and the endwall. Ar, Bi, are 0.5, 0, respectively. The height of liquid d is $2R\times$Ar with $R = 2.5[mm]$. The grid pints of $40 \times 24 \times 48$ (r $\times$ θ $\times$ z) is used in these simulations. In the case 1, the comparison of a liquid bridge with the statically straight surface in microgravity is performed. In the case 2, the result of simulation in a liquid bridge with the statically straight cylinder taken into account the effect of gravity is validated. In the case 3, the result of simulation in a liquid bridge with the statically deformed free surface is compared with that of LSA.

Table 4: The parameters for comparison with linear stability analysis.

	$Case1$	$Case2$	$Case3$
$surface\ shape$	$cylinder$	$cylinder$	$deformed(\alpha = 72)$
Pr	4.38	4.38	4.00
Gr	0	$8.97 \times 10^4 \times d^2 \times Re$	0

Table 5 shows the comparison with the results performed by LSA. In all case, the critical Re are compared with the result performed by LSA. The result of case 3 is in good agreement with that of LSA. In the cases 1 and 2, the value of critical Re is a little higher than the that of LSA. It is known that the critical value tends to decrease as the number of grid points increases [7]. Therefore, it is considered that the critical Re is higher than that of LSA because the grid points are coarse. In all case, the mode structures in liquid bridge are m=2. In the case of Ar=0.5, these mode structures agree with the structures obtained by LSA. The validity of the present program is confirmed through these examinations.

Table 5: The results of comparison with the linear stability analysis.

	$Case1$		$Case2$		$Case3$	
	$Present$	LSA[7]	$Present$	LSA[7]	$Present$	LSA[7]
Re_c	990	950	1090	970	1150	1150

3.3 Dynamic free surface deformation

3.3.1 Code validation of 2-dimensional calculation

In consideration of the dynamic free surface deformation, the 2-D code gives an axisymmetric steady flow. This result is compared with our previous data by the code without the dynamic free surface deformation. The compared results have already well verified as mentioned above. The 5 mm diameter liquid column with an aspect ratio of 0.5 is employed. The parameters used in this 2-D numerical simulation are: Re = 800, Pr = 4.4, Ca = 1.65×10^{-3} and g = 0. Figure 24 shows that the axial velocity and the temperature variation with time. The monitoring point is the mid-height over the free surface. The results agree well with each other.

The comparison of the free surface shape without Marangoni convection with experimental results is made in Figs. 25, 26. The experimental result in Fig. 25 is the ones given by Nishino at Marangoni Modeling Research meeting. Figure 26 is the computational results with the same aspect ratio and diameter as in the Fig. 25. Silicone oil of 5cSt is used. According to Nishino's results, the free surface is concaved in 10 μm at the point 400 μm apart from the edge of the upper disk, while the surface is also convexed near lower disk with a volume ratio of 1.0. The surface shape is rather asymmetry in upper and lower regions. A preliminary calculation with volume ratio gave symmetric surface shape. So, another volume ratio has been assumed. With volume ratio of 1.08, the present numerical analysis is in good agreement with the experiment. This difference can be acceptable within a range of an experimental error.

3.3.2 Code validation of 3-dimensional calculation

In the previous algorithm, the free surface shape was determined owing to the stress balance on the surface and resultant velocity variation with iterative calculation. The iteration requires a long calculation time. So an algorithm was modified to accelerate as Fig. 7. The temporary velocity and the shape of liquid bridge are calculated separately, and the flow field is replaced to fit to a new coordinate. Finally, the pressure is calculated using to the revised flow field. By this modification, the program can run much faster, and more robustly.

Next, Fig. 27 indicates the axial velocity and the temperature variation compared with our numerical result for the fixed surface. The monitoring point is mid-height. The present result can be compared for the condition of steady, non-oscillatory flow. Acetone (Pr = 4.4) is used in this calculation under the zero gravity. The symbol indicates the present result, and the line is the numerical one without surface deformation by our group. The 3-D results also agree well with the non-deformed results.

Figure 28 indicates the free surface shape without Marangoni convection. The blue line represents the experimental result given by from Nishino. The experimental conditions are: 5cSt of silicone oil as the test fluid, D=5mm, aspect ratio is 0.5, volume ratio is 1.048. The figure shows that the difference between experiment and numerical simulation is enough small and maximum difference is less than 5 %. Espesially, the maximum and minimum deflection points agree well each other.

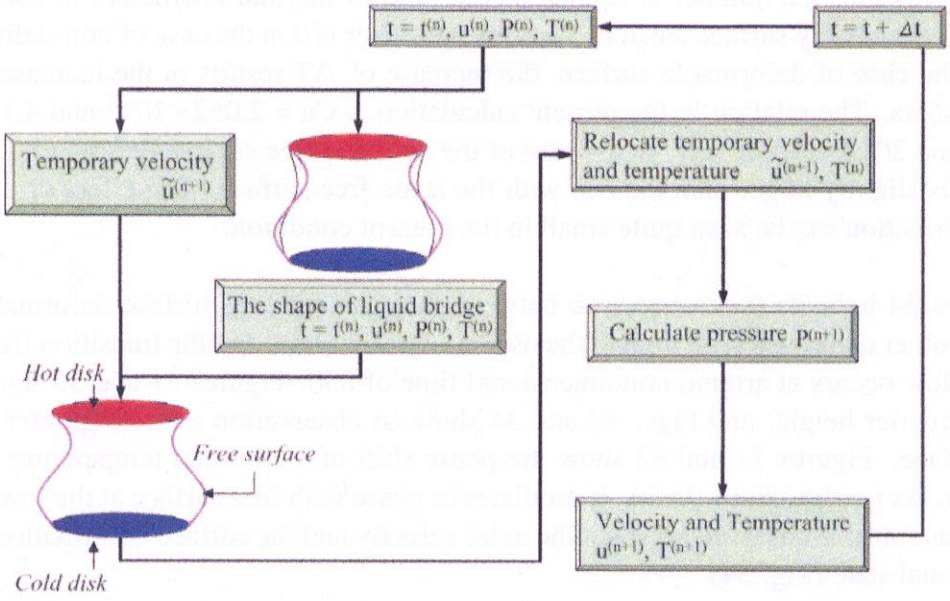

Figure 7: Algorithm of 3-dimensional code

3.3.3 Results of the 3-dimensional simulation

The critical Re number is calculated to investigate the effect of the dynamic free surface deformation for the critical condition. The black line in Fig. 29 indicates the absolute azimuthal velocity variation in each Re number without the dynamic free surface deformation under zero gravity. The test fluid is Acetone(Pr=4.4). We calculated in various Re numbers as given in Table 6.

Table 6: Re number

Re :	1000	1300	1500	2000

We can see that the azimuthal velocity increases gradually at Re = 2000. From the growth rate of the azimuthal velocity obtained in this figure, the critical Re number can be estimated, because the growth rate of 0 means the critical point. From the comparison between the growth rates in several Re numbers, the critical Re number can be estimated as 1020 (Fig. 30). Kulhmann's group reported that the critical Re number is about 950 in this case from their linear stability analysis. This difference may be attributed to the rather coarse mesh of $30 \times 20 \times 30$ (r $\times$ θ $\times$ z) in the present calculation. An additional calculation with a large grid number of $50 \times 40 \times 60$ has given a more stable results. This supports the above consideration. Then the angular velocity ω is compared. Our angular velocity is 31 while their theoretical result is 29 as shown in Table 7. So, both are in a fairly good agreement.

Table 7: The angular velocity compared with LSA

Present Result	31
Linear Stability Analysis	29

As for the liquid bridge with dynamic free surface deformation, the azimuthal velocity variation is shown as blue line in Fig. 29. The influence of Ca number is one of important parameters for surface deformation. Ca number is defined as the ratio of thermal coefficient of surface tension times delta T divided by surface tension. That is Ca number is 0 in the case of non-deformed liquid bridge. In the case of deformable surface, the increase of ΔT results in the increase of both Re and Ca numbers. The relation in the present calculation is Ca = 2.062×10^{-3} and 4.117×10^{-3} at Re = 1000 and 2000, respectively. In the case of the dynamic free surface deformation, the critical Re number is slightly larger than the one with the static free surface. The effect of dynamic free surface deformation can be seen quite small in the present condition.

Figures 31 $\sim$ 34 indicate the comparison between the dynamic free surface deformation and the variation of other quantities with time in the oscillatory flow state, and the transition from pulsative to rotation flow occurs at around nondimensional time of 850. Figures 31 and 33 show an observation at a quarter height, and Figs. 32 and 34 show an observation at three quarter height over the free surface. Figures 31 and 32 show the phase shift of π between temperature and surface deformation. As for the axial velocity, it oscillates in phase with free surface at the lower part (Fig. 33). The phase shift is observed between the axial velocity and the surface deformation, especially in the rotational state (Fig. 34).

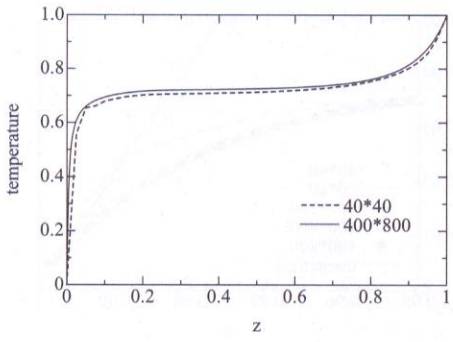

Figure 8: The distribution of the temperature on the free surface.

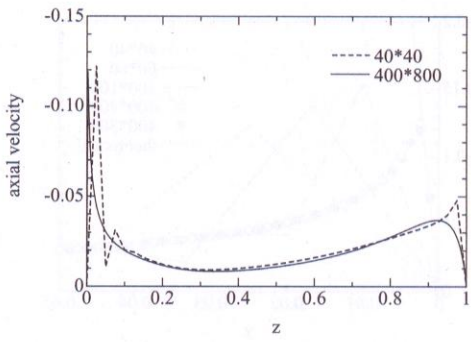

Figure 9: The distribution of the axial velocity on the free surface.

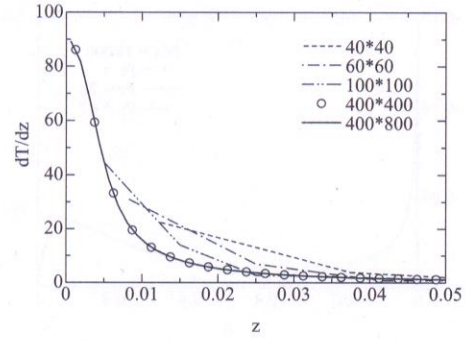

Figure 10: The distribution of the temperature gradient at the cold corner.

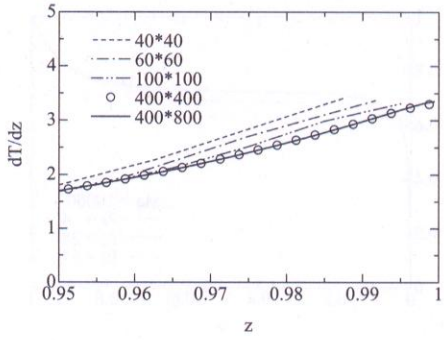

Figure 11: The distribution of the temperature gradient at the hot corner.

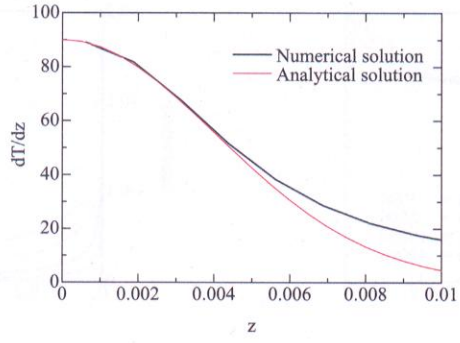

Figure 12: The distribution of the temperature gradient resolved analytically and numerically.

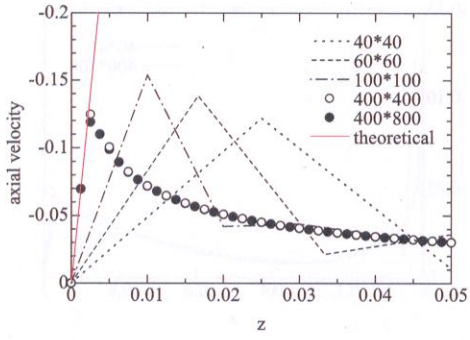

Figure 13: The distribution of the axial velocity at the cold corner.

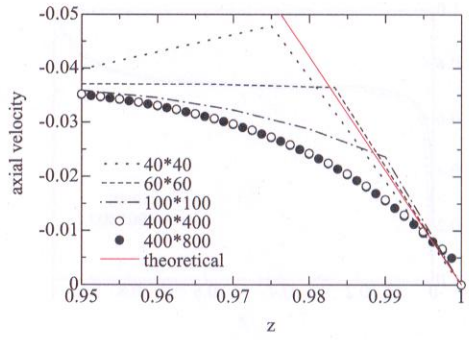

Figure 14: The distribution of the axial velocity at the hot corner.

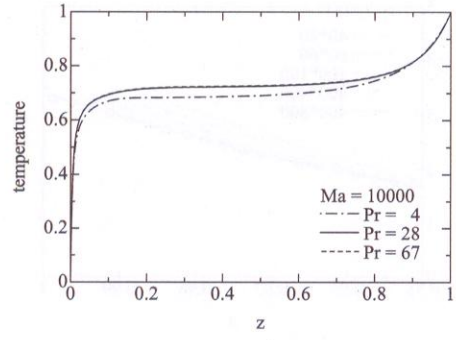

Figure 15: The distribution of the temperature on the free surface.

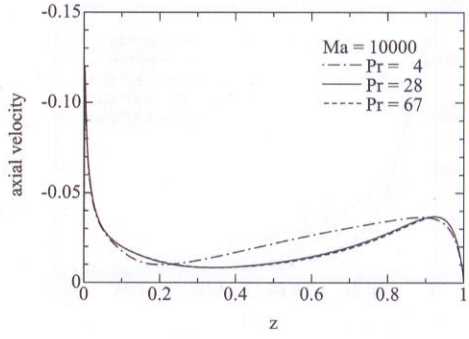

Figure 16: The distribution of the axial velocity on the free surface.

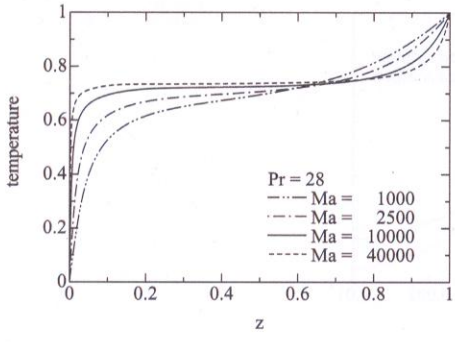

Figure 17: The distribution of the temperature on the free surface.

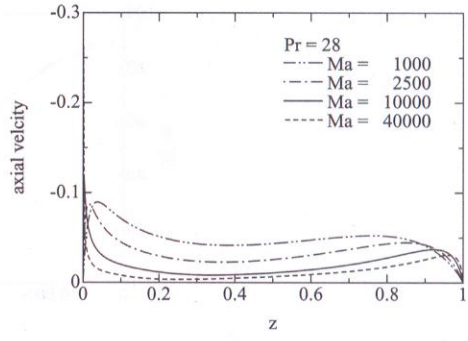

Figure 18: The distribution of the axial velocity on the free surface.

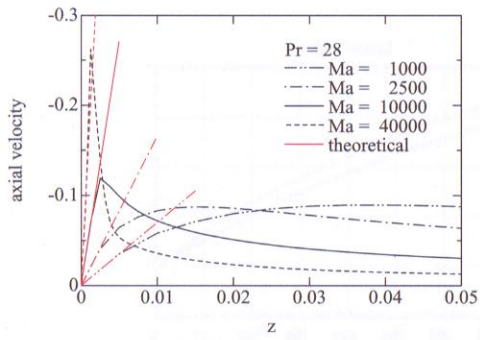

Figure 19: The distribution of the axial velocity at cold corner.

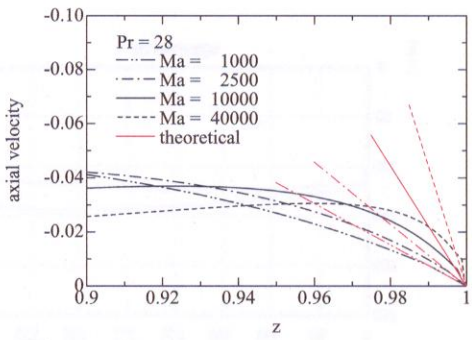

Figure 20: The distribution of the axial velocity at hot corner.

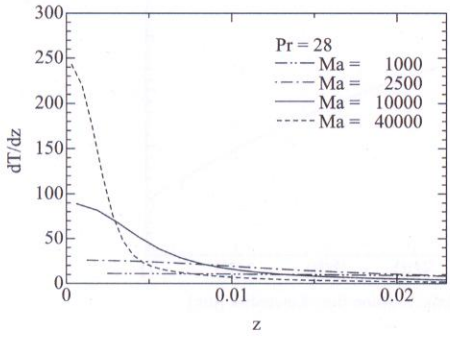

Figure 21: The distribution of the temperature gradient at cold corner.

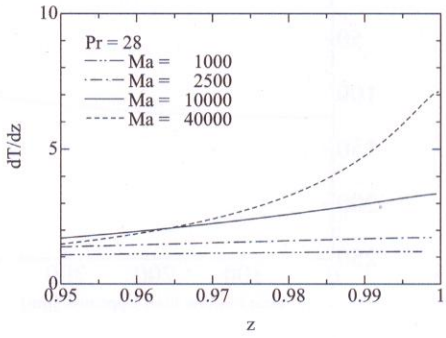

Figure 22: The distribution of the temperature gradient at hot corner.

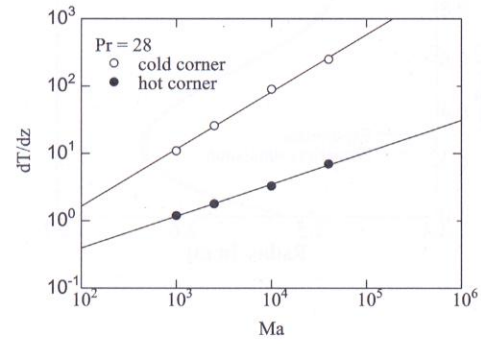

Figure 23: The Ma vs. the temperature gradient.

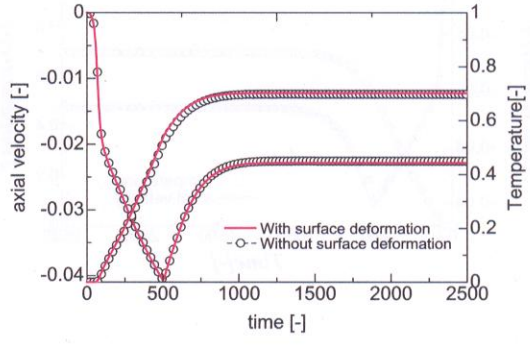

Figure 24: Axial velocity and temperature variation(2-D)

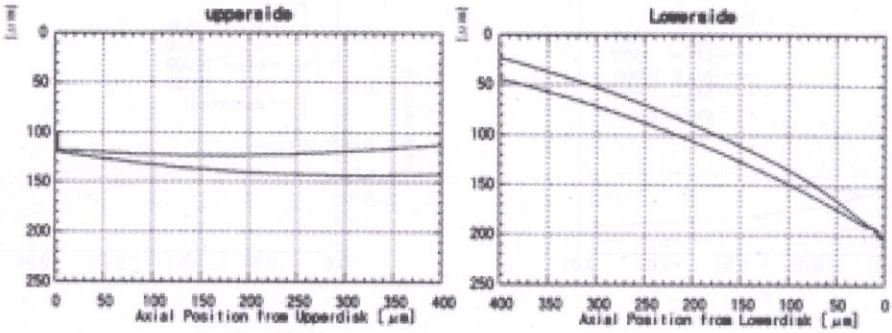

Figure 25: The free surface shape (Experiment)

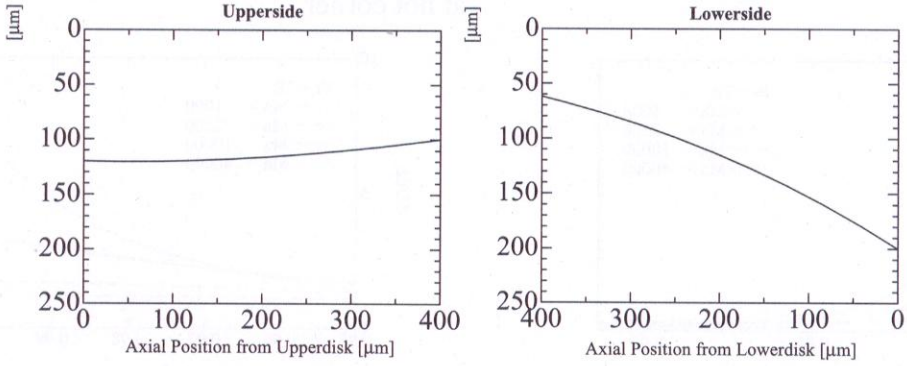

Figure 26: The free surface shape (Numerical Simulation)

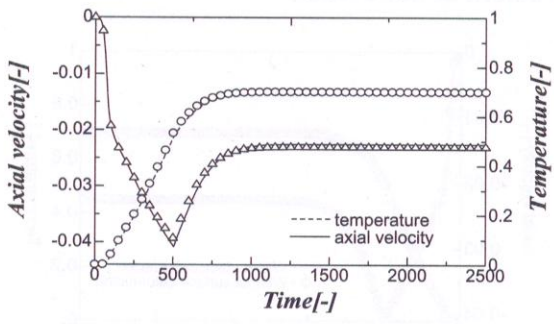

Figure 27: Axial velocity and temperature variation at the mid-height (3-dimension)

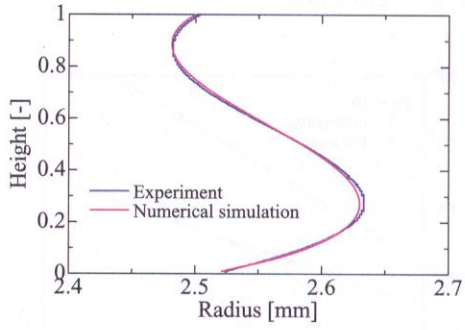

Figure 28: The shape of liquid bridge (3-dimension)

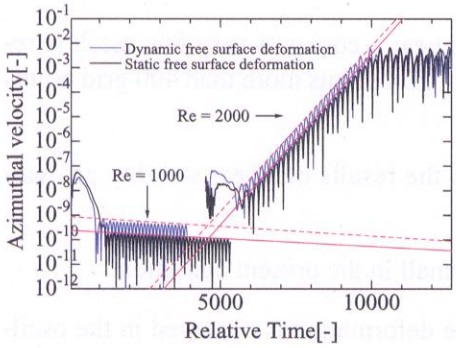

Figure 29: The azimuthal velocity variation in several Re number

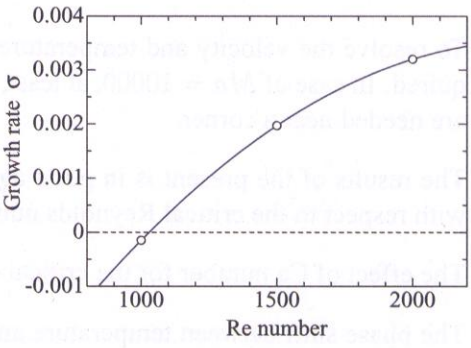

Figure 30: The growth rate of the azimuthal velocity

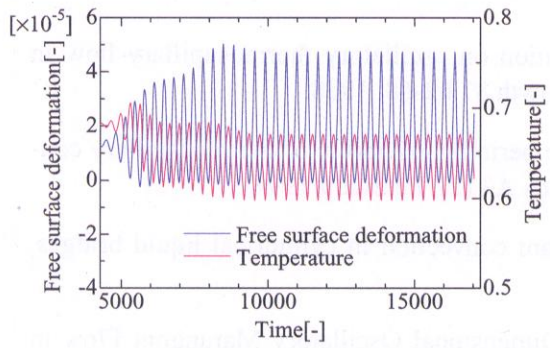

Figure 31: surface deformation vs. Temperature at the lower part

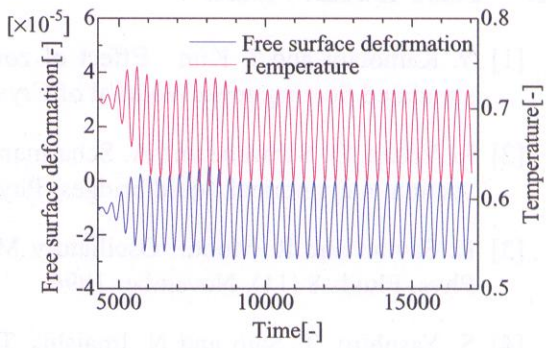

Figure 32: surface deformation vs. Temperature at the upper part

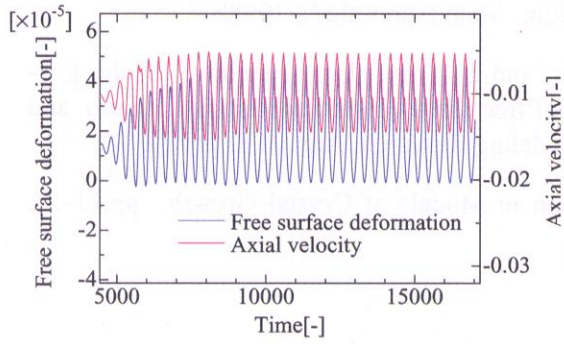

Figure 33: surface deformation vs. axial velocity at the lower part

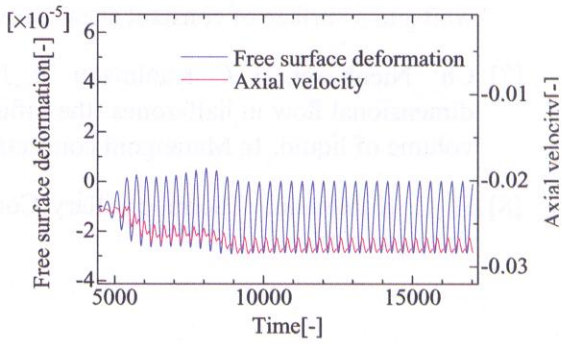

Figure 34: surface deformation vs. axial velocity at the upper part

4 CONCLUSIONS

(1) To resolve the velocity and temperature distributions near a corner, a very fine mesh is required. In case of $Ma = 10000$, at least, the number of grid points more than 400 grid points are needed near a corner.

(2) The results of the present is in good agreement with the results of linear stability analysis with respect to the critical Reynolds number.

(3) The effect of Ca number for the critical condition is small in the present condition.

(4) The phase shift between temperature and free surface deformation is observed in the oscillatory flow state. As for the axial velocity, the phase shifts is observed in the rotating flow state.

5 REFERENCES

[1] Y. Kamotani and J. Kim. Effect of zone rotation on oscillatory thermocapillary flow in simulated floating zones. Journal of Crystal Growth 87 62-68, 1988.

[2] R. Veltan, D. Schwabe and A. Scharmann. The periodic instability of thermocapillary convection in cylindrical liquid bridges. Phys. Fluids A3 (2), February 1991.

[3] R. Savino and R. Monti. Oscillatory Marangoni convection in cylindrical liquid bridges. Phys. Fluids 8 (11), November 1996.

[4] S. Yasuhiro, T. Sato and N. Imaishi. Three Dimensional Oscillatory Marangoni Flow in Half-zone of $Pr = 1.02$ Fluid. Microgravity sci. technol. x/3 (1997).

[5] D. Canright. Thermoocapillary flow near a corner. Phys. Fluids 6 (4), Aprile 1994.

[6] H. C. Kuhlmann, Ch. Nienh¨ser, and H. J. Rath. The local flow in a wedge between a rigid wall and a surface of constant shear stress. J. Eng. Math.(submitted), 1998b.

[7] Ch. Nienh¨ser, H .C. Kuhlmann, H. J. Rath, and S. Yoda. Linear stability of the tow-dimensional flow in half-zones: the influence of free surface heat transfer, aspect ratio, and volume of liquid. In Marangoni convection Modeling Research, Annual Report, 2000.

[8] H. C. Kuhlmann. Thermocapillary Convection in Models of Crystal Growth. pp.11-18, Springer 1999.